LRRK2 regulates synaptic function through BDNF signaling and actin cytoskeleton

Giulia Tombesi[1], Shiva Kompella[2], Giulia Favetta[1], Chuyu Chen[3], Yibo Zhao[4], Martina Sevegnani[5], Antonella Marte[6,11], Ilaria Battisti[7], Ester Morosin[1], Marta Ornaghi[8], Lucia Iannotta[1], Nicoletta Plotegher[1,9], Laura Civiero[1,9,10], Franco Onofri[6,11], Britta J Eickholt[8], Giovanni Piccoli[5], Giorgio Arrigoni[7], Dayne Beccano-Kelly[2,CA], Claudia Manzoni[4], Loukia Parisiadou[3] and Elisa Greggio[1,9,CA]

Author affiliations:

[1]Department of Biology, University of Padova, Italy
[2]School of Pharmacy and UK Dementia Research Institute, Cardiff University UK
[3]Northwest University, Chicago, USA
[4]School of Pharmacy, University College London, UK
[5]CIBIO, University of Trento, Italy
[6]Experimental Medicine, University of Genova, Italy
[7]Department of Biomedical Sciences, University of Padova, Italy
[8]Institute for Biochemistry, Charité Universitätsmedizin Berlin, Berlin, Germany
[9]Centro Studi per la Neurodegenerazione (CESNE), University of Padova, Italy
[10]IRCCS San Camillo Hospital, Venice, Italy
[11]IRCCS, Ospedale Policlinico San Martino, Largo Rosanna Benzi 10, 16132, Genova, Italy

Correspondence to: elisa.greggio@unipd.it or Beccano-KellyD@cardiff.ac.uk

Running title: LRRK2, BDNF and synaptic cytoskeleton

Keywords: Parkinson's disease, LRRK2, actin cytoskeleton, drebrin, BDNF, synapse

Abstract

Parkinson's disease (PD) is a multisystemic disorder that manifests through motor and non-motor symptoms. Motor dysfunction is the most debilitating and it is caused by the degeneration of dopamine-producing neurons in the substantia nigra pars compacta (SNpc). A body of evidence indicates that synapse demise precedes by years neuronal death. Still, early synaptic dysfunctions in PD are poorly deciphered.

Here we combined literature metanalysis, proteomics and phosphoproteomics with biochemical, imaging and electrophysiological measurements in neurons, brains and synaptosomes from knockout and knockin mouse models, as well as human iPSC-derived neurons associated with the PD-kinase LRRK2.

We show that phosphorylation of LRRK2 at Ser935, which controls LRRK2 subcellular localization, rapidly increases upon brain-derived neurotrophic factor (BDNF) stimulation of differentiated SH-SY5Y cells and primary mouse neurons. Affinity-purification coupled with mass spectrometry (AP-MS/MS) analysis revealed that LRRK2 interactome is significantly reshaped upon BDNF stimulation, with an interconnected network of actin cytoskeleton-associated proteins increasing their binding to LRRK2. Accordingly, LRRK2 knockout neurons exhibit decreased TrkB signaling and fail to induce BDNF-dependent spinogenesis. *In vivo*, one-month old *Lrrk2* knockout mice display defects in spine maturation, a phenotype that disappears with age. In human iPSC-derived cortical neurons, BDNF increases the frequency of miniature excitatory post-synaptic currents (mEPSC) in wild-type but not in the presence of LRRK2 knockout, functionally supporting a distinctive role of LRRK2 in BDNF-synaptic signaling. Finally, Lrrk2 G2019S PD mutant synaptosomes display differentially phosphorylated proteins enriched in categories related to postsynaptic structural organization.

Taken together, our study discloses a critical function of LRRK2 in BDNF-dependent synaptic processes and identifies the postsynaptic actin cytoskeleton as a convergent site of LRRK2 pathophysiological activity.

Introduction

Synaptic damage and connectome dysfunction are emerging as early pathological events preceding neurodegeneration and the manifestation of clinical symptoms in multiple neurodegenerative disorders, including Parkinson's disease (PD).[1–5] PD is an age-related motor disorder for which no cure is available. The motor symptoms typically manifest as a consequence of the progressive loss of the dopaminergic neurons of the Substantia Nigra pars compacta (SNpc) projecting to the striatum.[6] The degeneration of the nigrostriatal projections precedes the loss of the dopaminergic cell bodies in the SNpc and synaptic failure may be the triggering cause of axonal deterioration.[5,7] Pre- and postsynaptic alterations were described in PD animal models.[5] For example, PD pathology was reported as associated with an evident striatal spine loss, that appeared to be correlated with the degree of dopamine denervation prevalently due to glutamate excitotoxicity in striatal neurons.[8,9]

Accumulating evidence indicate that more than half of the causative genes and risk factors for PD have a function at the synapse. Mutations in *LRRK2* gene represent the most common cause of autosomal dominant late onset familial PD and variations around *LRRK2* locus increase lifetime risk for PD.[10] Pathogenic mutations are clustered into the enzymatic core of the LRRK2 protein, composed by a Roc/GTPase and a kinase domain, bridged by a COR scaffold.[11–13] The most frequent mutation (G2019S) located in the kinase domain results in a protein with a gain of kinase activity, associated with increased cellular toxicity.[11] Previous data from our team and other laboratories suggested that LRRK2 sits at the crossroads between cytoskeletal dynamics and vesicular trafficking. LRRK2 activity seems to be mediated via interactions with a plethora of cytoskeletal and vesicle-associated proteins and via phosphorylation of a subset of Rab GTPases.[14,15] LRRK2 subcellular localization is dynamically controlled by phosphorylation/dephosphorylation of a cluster of N-terminal serine residues (e.g. Ser935 and Ser910), which determines 14-3-3 protein binding.[16] Phosphorylation of LRRK2 Ser935 and Ser910 is regulated by multiple kinases, including casein kinase 1 alpha (CK1a), IKKs and protein kinase A (PKA),[17–19] and serves as a scaffold for 14-3-3 protein binding and LRRK2 subcellular localization.[16,20] In immune cells, extracellular signals such as Toll-like receptor 4 (TLR4) agonists stimulate LRRK2 Ser935 and Ser910 phosphorylation to positively modulate immune-related responses.[17,21] In contrast, the extracellular signals that orchestrate Ser935 phosphorylation in neurons are still unknown. However, the ability of the neurons to relocate LRRK2 to the synapse is particularly important as LRRK2 was suggested

to provide the scaffold for the assembly of the signalling cascade effectors to sustain the main synaptic functions.[14] LRRK2 has been shown to regulate synaptic vesicles cycling at the presynaptic site through interaction and phosphorylation of a panel of pre-synaptic proteins,[22] such as NSF,[23] synapsin I,[24] EndophylinA,[25] synaptojanin-1[26] and DNAJC6/Auxilin.[27] Interestingly, recent literature supports a role for LRRK2 in the dendritic spine compartment, where it was suggested to influence receptor traffic,[28] spine morphology and functionality in developing brains.[29–31]

Here, starting from the observation that brain derived neurotrophic factor (BDNF) stimulates LRRK2 Ser935 phosphorylation in neurons, we used unbiased protein-protein interaction (PPI) and phosphoproteomic investigations to disclose a novel function of LRRK2 in regulating actin-dependent synaptic dynamics in complementary neuronal models.

Results

BDNF treatment rapidly increases LRRK2 phosphorylation at Ser935

Neurotrophic factors plastically shape neuronal activity by binding to their cognate receptor tyrosine kinases.[32] Brain-derived neurotrophic factor (BDNF) is particularly important to modulate neurotransmission in the cortico-striatal circuitry.[33] This circuitry is relevant for PD and presents with the highest LRRK2 expression in comparison with the rest of the brain.[34,35] To address whether LRRK2 Ser935 phosphorylation is stimulated by BDNF, we prepared primary mouse cortical neurons from C57BL/6J wild-type mice and stimulated them with 100 ng/ml of BDNF at days in vitro 14 (DIV14) when synapses are fully functional (Fig. 1A) and LRRK2 expression is detectable.[36] Western blot analysis revealed a rapid (5 mins) and transient increase of Ser935 phosphorylation after BDNF treatment (Fig. 1B and 1C). Of interest, BDNF failed to stimulate Ser935 phosphorylation when neurons were pretreated with the LRRK2 inhibitor MLi-2, indicating that either LRRK2 kinase activity controls the upstream kinases activated by BDNF or that the binding with MLi-2, a type I inhibitor, locks the kinase in a conformation that favors dephosphorylation/hinders phosphorylation during the stimulus.[37]

To gain mechanistic insights into the effects of BDNF stimulation on LRRK2 function, we differentiated neuroblastoma SH-SY5Y cells with 10 μM retinoic acid (RA) treatment for 6 days[38] and measured BDNF response by monitoring Tropomyosin receptor kinase B (TrkB) levels and phosphorylation of AKT and ERK1/2, two major downstream effector pathways of BDNF/TrkB signaling (Fig. 1D).[39] Expression of TrkB is undetectable in undifferentiated SH-SY5Y cells, whereas RA-differentiation boosts TrkB expression (Fig. 1E). Accordingly, differentiated SH-SY5Y cells respond to 100 ng/ml BDNF stimulation, as evidenced by increased phosphorylation of ERK1/2 and AKT (Fig. 1F-G). Strikingly, BDNF treatment stimulates Ser935 phosphorylation of endogenous LRRK2 with a phosphorylation kinetics overlapping with that observed in primary neurons (Fig. 1H). These findings support RA-differentiated SH-SY5Y as a valuable model to investigate a novel BDNF-LRRK2 pathway.

BDNF promotes LRRK2 interaction with actin cytoskeleton components enriched at the postsynapse.

To clarify the implications of BDNF-mediated Ser935 phosphorylation on LRRK2 neuronal function, we used affinity purification coupled with mass spectrometry (AP-MS/MS). As the yields of endogenous LRRK2 purification were insufficient for AP-MS/MS analysis, we generated polyclonal SH-SY5Y cells stably expressing GFP-LRRK2 wild-type or GFP control (Supplementary Fig. 1). Then we used GFP-trap purification to isolate GFP or GFP-LRRK2 from RA-differentiated cells unstimulated or stimulated with BDNF for 15 mins prior to MS analysis. The unstimulated LRRK2 interactome (GFP-LRRK2 vs. GFP) is large (207 significant hits) and consistent with previous computational analysis of LRRK2 PPIs.[40,41] In particular, we confirmed interactions with known LRRK2 binders including 14-3-3 proteins, cytoskeletal proteins and protein translation factors (Supplementary table 1). Since BDNF is synaptically released and influences pre- and post-synaptic mechanisms, we used SynGO[42] to identify synaptic LRRK2 interactors. About one-third (35%) of LRRK2 PPI under unstimulated conditions are SynGO annotated genes; among them, 33% are presynaptic proteins and 66% are post-synaptic proteins (Fig. 2B). The most significant enriched categories were pre- and post-synaptic ribosome and post-synaptic actin cytoskeleton (Fig. 2B).

We next compared unstimulated vs. BDNF-stimulated LRRK2 interactome. As shown in Fig. 2C, 15 minutes of BDNF stimulation reshapes LRRK2 PPI, with a group of interactors

increasing binding with LRRK2 (blue dots) and another group decreasing binding (orange dots). The inclusion criteria were either *P* value < 0.05 and fold change FC > 0.5 | FC < -0.5 or FC > 1 | FC < -1 independently from the *P* value. In this way, we increased the discovery power for gene ontology analysis. SynGO gene ontology revealed that 10 out of 19 hits with increased binding after BDNF (BDNF(+)) and 21 out of 50 hits with decreased binding (BDNF(-)) are synaptic proteins (Fig. 2C inset). Among synaptic interactors, the BDNF(+) binders are enriched in actin-cytoskeleton-related GO:BP categories while the BDNF(-) binders are enriched in protein translation GO:BP categories (Fig. 2D). Furthermore, 80% of synaptic BDNF(+) LRRK2 binders (DBN1, ARPC2, ACTR2, ACTR3, CFL1, CALD1, ACTN1, FLNA) and 62% of synaptic BDNF(-) binders (RPS2, RPS4X, RPS7, RPS9, RPS11, RPS13, RPS15A, RPL13, RPL23, RPL26, RPL27A, TUFM, EEF1A2, PCBP1) form functional and physical interaction networks (Fig. 2F-E).

To validate these findings, we performed western blot analysis on the AP samples analyzed by MS. We selected drebrin, encoded by *DBN1*, because it sits at the center of the BDNF(+) network (Fig. 2E, inset SynGO) and, in DIV14 primary neurons, it colocalizes with PSD95, a postsynaptic marker (Fig. 2G), confirming previous observations.[43] As predicted, BDNF treatment increases LRRK2:drebrin interaction by ~2 fold (Fig. 2H-I and Supplementary Fig. 2). We conclude that BDNF stimulation engages LRRK2 into actin cytoskeleton dynamics through physical association with actin-related proteins. This stimulus-dependent function may be relevant at the postsynaptic site (Fig. 2B and 2G). Our findings also suggest that a pool of LRRK2 binds protein translation factors under unstimulated conditions and translocates to the actin-cytoskeleton upon BDNF-TrkB signaling.

An actin-synaptic cluster from a literature-based LRRK2 PPI network

We recently investigated the molecular environment surrounding LRRK2 specifically by constructing the protein-protein interaction (PPI) interactome around LRRK2 based on PPIs derived from peer reviewed literature. After filtering the LRRK2 PPIs for reproducibility (keeping only those interactions that have been reported at least twice in literature or at least replicated with 2 different interaction detection methods) we obtained the interactions linking across the LRRK2 interactors thus effectively building the LRRK2 protein interaction network ($LRRK2_{net}$) which describes the protein milieu around LRRK2 in the cellular context (see Zhao

et al.[44] for details). The $LRRK2_{net}$ was topologically analyzed to identify the portions (clusters) of the network that are more densely connected locally in comparison with the overall connectivity of the entire network as these topological clusters are likely to represent functional units.[45] Among the 11 topological clusters identified in Zhao *et al.*[44], we further elaborated on one cluster in particular, containing 41 genes (Fig. 3A) and found that it exhibited significantly GO-BP enriched terms into semantic categories related to: actin polymerization (16 GO-BP terms), synaptic vesicles (5 GO-BP terms), postsynaptic actin-cytoskeleton (2 GO-BP terms), lamellipodium (6 GO-BP terms), cell-neuron projection/size (2 GO-BP terms), DNA recombination/repair (4 GO-BP terms) and uncategorized (6 GO-BP terms) (Fig. 3B and Supplementary table 2). Out of the 41 proteins forming the cluster, 23 are proteins associated with the actin cytoskeleton including the 4 larger nodes (where the dimension of the nodes is directly proportional to the node degree/connections within the network): DBN1/drebrin, CAPZA2 and LIMA whose association with LRRK2 was identified in Meixner *et al.*[46] and IQGAP1 identified in Liu *et al.*[47] (Fig. 3C). Given the overrepresentation of synapse-related GO-BP terms, we further performed GO functional enrichment using SynGO and mapped 16 synaptic proteins within the cluster (Fig. 3D). Strikingly, DBN1/drebrin is a key protein in the cluster, as it engages in multiple interactions (16 edges) and sits at the interface between the nodes involved in GO:BPs functions related to the actin cytoskeleton (blue-colored nodes) and to the synapse (red-colored nodes) (Supplementary Fig. 3). Taken together, these findings corroborate our experimental interactome network (Fig. 2), supporting the existence of an actin-synaptic LRRK2 network, which appears dynamically shaped by BDNF stimulation.

BDNF-mediated signalling and spinogenesis is impaired in LRRK2 knockout neurons.

Based on Ser935 phosphorylation and AP-MS/MS analysis indicating that LRRK2 responds to BDNF (Fig. 1 and 2), we next asked whether LRRK2 knockout could affect BDNF/TrkB downstream cascades. To this end, we generated LRRK2 knockout (KO) SH-SY5Y cells with CRISPR/Cas9 editing (Supplementary Fig. 4), differentiated them with RA and assessed their response to BDNF stimulation. While application of BDNF increases AKT and ERK1/2 phosphorylation in naïve SH-SY5Y, as expected, LRRK2 KO cells exhibit a remarkably weaker response (Fig. 4A-B). These results indicate that LRRK2 acts downstream of TrkB and

upstream of AKT and ERK1/2, in line with its rapid and transient phosphorylation kinetic upon BDNF stimulation (Fig. 1B-C).

Likewise, *Lrrk2* WT and KO primary cortical neurons at DIV14 were stimulated with BDNF at different timepoints. Similar to differentiated SH-SY5Y cells, *Lrrk2* WT neurons responded to BDNF by rapidly increasing Akt and Erk1/2 phosphorylation, whilst KO neurons exhibited a significantly reduced phosphorylation of Akt and Erk1 (Fig. 4D-E). Of note, 90 mins of Lrrk2 inhibition (MLi-2) prior to BDNF stimulation did not prevent phosphorylation of Akt and Erk1/2, suggesting that LRRK2 participates in BDNF-induced phosphorylation of Akt and Erk1/2 independently from its kinase activity but dependently from its ability to be phosphorylated at Ser935 (Fig. 4C-D and Fig. 1B-C).

Considering that (i) BDNF induces dendritic spine formation, maturation and structural plasticity,[48,49] (ii) BDNF(+) LRRK2 interactors are actin-related proteins enriched at the postsynapse (Fig. 2) and (iii) loss of LRRK2 causes reduced phosphorylation of BDNF/TrkB downstream kinases AKT and ERK1/2 (Fig. 4), we next evaluated BDNF-induced spine formation in the presence or absence of Lrrk2. Primary cortical neurons were transfected with GFP filler at DIV4 and treated with BDNF for 24 h at DIV13 (Fig. 4E). Consistent with previous findings,[50,51] BDNF treatment significantly increased the density of dendritic spines in WT cultures ($P < 0.001$) (Fig. 4F-G). In contrast, BDNF failed to induce spinogenesis in *Lrrk2* KO neurons. These data support a crucial role for LRRK2 in spine morphogenesis in response to BDNF.

Dendritic spine maturation is delayed in *Lrrk2* knockout mice.

Based on the *in vitro* results indicating that BDNF stimulates the recruitment of LRRK2 through Ser935 phosphorylation and binding to actin-cytoskeleton to promote spinogenesis, we next investigated whether loss of *Lrrk2 in vivo* results in dendritic spine defects. During development, dendritic spines are highly dynamic, with a rate of extension and retraction that allows proper and accurate synapse formation and neuronal circuit assembly.[52] By the adulthood, dendritic spines formation, motility, and pruning decrease reaching a relatively stable number of protrusions.[53] Since spines dynamics vary according to the stage of brain development, we performed a longitudinal analysis of young (1 month-old), adult (4 month-old) and aged (18 month-old) *Lrrk2* WT and KO mice in order to capture any age-dependent

defect (Fig. 5A). We focused on the dorsal striatum, a region highly enriched in SPNs that receives excitatory afferents from the cortex and dopaminergic modulation from the SNpc. This region is relevant in the prodromal stages of PD neurodegeneration[54] and expresses high levels of LRRK2[34,55]. Moreover, several studies showed a key role of LRRK2 in shaping the structure and function of excitatory synapses in the striatum.[29,30,56,57] We evaluated the number and morphology of dendritic spines using Golgi-Cox staining (Fig. 5B). The total number of protrusions varied across ages, but there were no differences between the two genotypes (Fig. 5C). Instead, the width and the length of the protrusions were reduced in 1 month-old Lrrk2 KO striata with respect to WT. Specifically, the average neck height was 15% shorter and the average head width was 27% smaller, meaning that spines are smaller in *Lrrk2* KO brains. No differences were observed at 4 and 18 months of age (Fig. 5C). We then classified the morphology of spines into four categories: filopodia and thin protrusions (immature spines) and mushroom and branched protrusions (mature spines). One month-old *Lrrk2* KO animals exhibit a reduced number of filopodia and an increased quantity of thin protrusions, suggesting that loss of Lrrk2 may favor this transition. Instead, the proportion of mature spines (mushroom and branched) remained unaltered. No differences were observed in older mice (Fig. 5D).

Since the overall width/height of *Lrrk2* KO protrusions is reduced (Fig. 4C), we next analyzed the postsynaptic ultrastructure using electron microscopy. To increase the experimental power, we used a separate group of animals. We measured the postsynaptic density (PSD) length as it directly correlates with the amount of postsynaptic receptors and signaling proteins, thus providing an indication of the synaptic strength (Fig. 5E). PSD is significantly shorter in 1 month-old *Lrrk2* KO animals compared to WT ($P < 0.001$), while no differences in PSD length are observed in 18 month-old KO mice (Fig. 5F). Taken all these data together, we conclude that subtle postsynaptic maturation defects are present in the striatum of post-natal *Lrrk2* KO mice.

To establish whether loss of *Lrrk2* in young mice causes a reduction in dendritic spines size by influencing BDNF-TrkB expression, we measured *Bdnf* and *TrkB* transcripts, as well as *Psd95* and *Shank3*, two major postsynaptic scaffolds. Neither *Bdnf* nor *TrkB* expression is altered in the striatum, cortex or midbrain of 1-month old Lrrk2 KO as compared to WT mice (Fig. 5G), supporting a mechanism whereby LRRK2 is influenced by BDNF signaling, but the absence of LRRK2 does not affect *Bdnf* or *TrkB* expression. Instead - and as expected - *Psd95* and *Shank3* expression is lower in *Lrrk2* KO mice and, interestingly, the effect is not limited to the striatum but is also found in the cortex and midbrain.

Given (i) the central role of *Dbn1*/drebrin in the LRRK2 synaptic network (Fig. 2-3), (ii) its key function as an actin regulatory protein and (iii) its expression highly enriched at dendritic spines (Fig. 2I), we assessed drebrin protein levels at the 3 stages of life in whole brain lysates. Of interest, drebrin expression is significantly lower in 1 month-old *Lrrk2* KO mice but not in older animals (Fig. 5H), further linking defective spine maturation with improper actin-dynamics in the absence of LRRK2.

Taken together, our results indicate that LRRK2 influences dendritic spines maturation in the developing brain.

Knockout of LRRK2 in human iPSC-derived cortical neurons prevents BDNF-dependent increase of spontaneous electrical activity.

To further explore the connection between LRRK2 and BDNF activity in a cell model more relevant for human disease, we differentiated human induced pluripotent stem cells (hiPSCs) into cortical neurons following established protocols.[58] Wild-type and isogenic LRRK2 knockout hiPSCs[59] were differentiated in parallel for 70 days (3 independent culture rounds per genotype), prior to subjecting them to patch clamp to assess spontaneous neurotransmitter release in the absence or presence of acute exposure to BDNF (24 hrs, 50 ng/ml) (Fig. 6A). Acute BDNF treatment led to a significant increase in the mean frequency of miniature post-synaptic excitatory currents (mEPSC) in WT cultures (vehicle: 0.16 ± 0.03 Hz, n=15, N=3; BDNF: 1.05 ± 0.25 Hz, n=10, N=3) (Fig. 6B, left). This is corroborated by the significant leftward shift in cumulative probability curves of interevent intervals (IEIs) between BDNF-treated neurons versus untreated neurons (Fig. 6B, right). In contrast, no significant change in mEPSC frequency of IEI was observed when KO neurons were stimulated with BDNF (pre-BDNF: 1.09 ± 0.21 Hz, n=11, N=3; post-BDNF: 1.11 ± 0.25 Hz, n=12, N=3) (Fig. 6C). BDNF treatment had instead no effect on the average peak amplitude in both genotypes (WT - vehicle: 11.00 ± 1.85 pA (n=14, N=3); BDNF 7.4 ± 0.77 pA (n=10, N=3); KO - vehicle: 10.42 ± 1.53 pA (n=11, N=3); BDNF 11.12 ± 1.76 pA (n=12, N=3)) (Fig. 6D-E). Of note, LRRK2 KO cultures appear to exhibit consistently higher mEPSC frequency (not amplitude) with respect to WT cultures (Fig. 6B-C, Supplementary Table1). As Lrrk2 KO in mouse display maturation abnormalities of dendric spines during development, it is possible that anomalous synaptic

maturation also occurs in LRRK2 KO hiPSCs. In this experimental paradigm, we conclude that BDNF mainly affects the presynapse rather than the postsynapse (unchanged mEPSC amplitude), likely increasing neurotransmitter release in WT neurons. Indeed, confocal imaging of synapses shows no increase in the total number of synapses under BDNF stimulation (Supplementary Fig. 5), thus pointing directly to an increase in release probability (P_r) of presynaptic neurotransmitter. Importantly, loss of LRRK2 blunts the positive effect of BDNF on synaptic transmission.

Phosphoproteome of Lrrk2^{G2019S} synaptosomes is enriched in postsynaptic structure organization SynGO terms.

Our data so far indicate that LRRK2 influences synaptic morphology and BDNF-dependent function by engaging in complex formation with actin-cytoskeleton elements. We then asked whether the kinase activity of LRRK2 may also play a role in these processes. To this end, we purified synaptosomes from WT and hyperactive Lrrk2^{G2019S} knockin (KI) mice and performed phosphopeptide enrichment and MS analysis (Fig. 7A). Synaptosomal preparations are highly enriched in pre- and postsynaptic components.[29] We identified 2957 phosphopeptides common between WT and Lrrk2^{G2019S} synaptosomes. Among them, 343 phosphopeptides showed a significant decrease or increase phosphorylation in Lrrk2^{G2019S} with respect to WT (Fig. 7B and Supplementary Table 3). The LRRK2 kinase substrates Rabs are not present in the list of significant phosphopeptides, likely due to the low stoichiometry and/or abundance. Next, by overlapping the list of proteins containing at least 1 significant phosphopeptide (267 proteins) (and with a human orthologue) with the list of AP-MS LRRK2 interactors identified in SH-SY5Y cells (207 proteins) (Fig. 7A-B), we found 5 proteins in common (CEP170, HSP90AB1, MAP1B, TUBA1A, and DBN1) highlighted with colored dots in the volcano plot (Fig. 7B). One hundred thousand random lists containing 207 proteins each (to mimic the AP-MS list) were overlapped with the 267 significant genes in the phosphoproteomic dataset resulting in a distribution of overlaps peaking around 2, indicating that 5 overlaps are not a random event. Four (CEP170, HSP90AB1, MAP1B and TUBA1A) were previously reported LRRK2 interactors.[16,60–63] Strikingly, DBN1/drebrin is a significant hit also in this dataset. Drebrin binding with actin is regulated by Cdk5-mediated phosphorylation at Ser142.[64] In our dataset however, the phosphorylation of this site is not affected by Lrrk2^{G2019S} activity, instead we observed a significant reduction of a peptide containing two phosphorylated residues (S385

and S387 in mouse and S337 and S339 in human drebrin), previously reported by multiple high throughput studies (https://www.phosphosite.org/homeAction). The lower phosphorylation of this drebrin peptide in Lrrk2^{G2019S} implies that the effect is indirect. Possible kinases phosphorylating these sites are Cdk5 and PKA (NetPhos 3.1 Server)[65,66], providing clues on regulatory mechanisms underlying LRRK2:drebrin binding.

Next, we performed GO analysis of differentially phosphorylated proteins using SynGO. Biological processes (BP) significantly enriched include synaptic vesicle cycle/exocytosis and postsynaptic structural organization (Fig. 7C). Enrichment by cellular components (CC) similarly indicates synaptic vesicles and postsynaptic density/cytoskeleton as enriched terms (Fig. 7D). This analysis confirms the established role of LRRK2 as a crucial regulator of synaptic vesicles cycle[22] and further support a previously underestimated function of LRRK2 in regulating postsynaptic structural plasticity.

Discussion

Understanding the early events that lead to synaptic dysfunction in PD is crucial to design effective therapeutic approaches. Previous work from our laboratories and other groups have shown that the PD-associated kinase LRRK2 regulates important synaptic processes.[67,68] At the presynapse, LRRK2 controls synaptic vesicles cycle through association with its WD40 domain[69–72] and phosphorylation of a panel of presynaptic proteins, including N-ethylmaleimide sensitive fusion (NSF)[23], synapsin I[24], auxilin[27], synaptojanin[26] and EndophylinA.[25] It has also been shown to regulate neurotransmitter release via modulation of presynaptic vesicular interacting proteins. At the postsynapse, LRRK2 plays key roles in shaping the function of excitatory synapses in the striatum.[29,30,56,57,68] However, the mechanisms underlying LRRK2 synaptic function are still poorly elucidated. In the present study we provide multiple lines of evidence that LRRK2 shapes dendritic spines morphology and synaptic function in response to BDNF neurotrophic stimulation, which promotes relocalization of LRRK2 to the actin-cytoskeleton in a phosphorylation-dependent manner.

There are several novel findings in our study. First, we identify BDNF as an extracellular stimulus increasing LRRK2 Ser935 phosphorylation in neurons. The phosphorylation kinetics are fast and transient, and both Lrrk2 KO neurons and differentiated SH-SY5Y LRRK2 KO

cells display reduced AKT and ERK1/2 downstream pathways activation, all consistent with LRRK2 positioned downstream of TrkB/BDNF and upstream of ERK1/2 and AKT. Using a literature-based network analysis of LRRK2 PPIs as well as AP-MS/MS in SH-SY5Y, we found that LRRK2 interacts with a highly interconnected cluster of actin and synaptic proteins, whose association increases after rapid (15 mins) BDNF stimulation. Moreover, loss of *Lrrk2* results in impaired BDNF-induced spinogenesis *in vitro* and delayed spine maturation *in vivo*, pointing to a mechanism whereby BDNF-mediated Ser935 phosphorylation engages LRRK2 into a macromolecular complex required to coordinate actin dynamics during postsynaptic structural plasticity. Accordingly, BDNF is key to reorganize the actin cytoskeleton during long term potentiation (LTP) through the action of Rho GTPases Rac1 and Cdc42.[73] LRRK2 was previously reported to interact with Rac1[74,75] and with other actin-related proteins.[46] Here we demonstrate that LRRK2 association with actin cytoskeleton in dendritic spines increases upon BDNF stimulation. We validated the BDNF-dependency of the interaction between LRRK2 and drebrin, an actin binding protein that promotes stable F-actin formation in dendritic spines.[43] We found that drebrin phosphorylation at Ser337/Ser339 is significantly lower in synaptosomes from hyperactive Lrrk2 G2019S mice, further strengthening the relevance of this interaction also in a pathological context. Loss of drebrin results in delayed synaptogenesis and inhibition of postsynaptic PSD95 accumulation, suggesting a key role in spine maturation.[43,76,77] During LTP, Ca^{2+} entry through N-methyl-d-aspartate (NMDA) receptors causes drebrin exodus from the spine compartment to allow actin monomers entrance and polymerization to increase the size of the cytoskeleton.[78] We postulate that LRRK2 may favor drebrin exodus at the shaft of the dendrite during plasticity processes. Actin remodeling during spine enlargement is also coordinated by the ARP2/3 complex, which is activated by binding to WAVE family proteins downstream of active Rac1.[79] Strikingly, we found that BDNF stimulates LRRK2 interaction with three out of seven subunits of the ARP2/3 complex (ACTR2, ACTR3 and ARPC2) and LRRK2 was reported to interact with WAVE proteins.[80] Altogether these findings, in agreement with our earlier study,[31] highlight a crucial role for LRRK2 in actin-based dendritic spine remodeling. Clearly, future studies should be directed at clarifying the precise molecular dynamics and kinetics of these processes.

Our data in human neurons differentiated from iPSCs further support an effect of LRRK2 in modulating neurotransmission in response to BDNF. Previous evidence has shown that LRRK2 modulates neurotransmitter release,[22] however our current findings imply that these changes

can be acutely altered by BDNF signalling with loss of LRRK2 removing this plastic ability to modulate synaptic function upon neurotrophic signaling.

Another interesting aspect disclosed here is a developmental phenotype characterized by defects in spine maturation as consequence of loss of LRRK2. Interestingly, this developmental abnormality is rescued with age. This is not surprising considering that the homologous kinase LRRK1 may compensate for LRRK2 deficiency, as suggested by the overt neurodegeneration observed in double *Lrrk1/Lrrk2* KO mice but absent in the single KO[81,82] and the redundant but not overlapping pattern of expression of the two kinases.[83] Indeed, striatal Lrrk2 expression in the rodent brain increases up to postnatal week 4,[31,55,83,84] while Lrrk1 transcript in this region is relatively stable during development.[55]

The pre- and postsynaptic roles of LRRK2 highlighted in KO models was further corroborated by the phosphoproteomic analysis of WT vs. mutant G2019S striatal synaptosomes, which revealed that LRRK2 kinase activity plays distinct functions in the regulation of synaptic vesicle cycle and in the organization of postsynaptic cytoskeleton and density. Accordingly, ultrastructural and expression analyses showed reduced postsynaptic density in 1 month-old *Lrrk2* KO mice. There is a tight connection between postsynaptic density organization/expansion and actin cytoskeleton. Interactions of the F-actin binding protein Abp1 with members of the Shank family, such as Shank3, serve as anchoring points for the dynamics of postsynaptic actin cytoskeleton.[85] Reduced expression of Shank3 and Psd95 in 1 month-old Lrrk2 mice further support these connections.

Several lines of evidence indicate that genetic, biochemical and cellular alterations of BDNF/TrkB signaling are linked to PD. At striatal synapses, BDNF/TrkB signaling enhances both dopamine and glutamate release and ERK1/2 activation.[86,87] BDNF is required for the establishment of the proper number and for the survival of dopaminergic neurons in the SNpc, [88,89] and presynaptic dopamine release in the striatum is enhanced by BDNF.[33] BDNF levels are lower in peripheral tissues, brain, and blood of sporadic PD patients.[90] Moreover, the V66M polymorphism modifies the risk of sporadic and mutant LRRK2-associated PD.[91,92] Decreased BDNF concentration in serum and brain correlates with an increased degeneration of dopaminergic neurons in PD[93] and with loss of striatal DA transporter (DAT) in patients with striatal dopaminergic neurodegeneration.[94] Thus, robust literature support deregulation of striatal BDNF signaling in PD. Future studies should be directed at investigating possible

deregulated mechanisms of BDNF signaling in G2019S mice and hiPSCs-derived neurons with G2019S mutation.

At the onset of PD, loss of dopaminergic axonal terminals largely exceeds loss of cell bodies,[4] implying that early synapse deterioration may be the trigger of axonal degeneration and, ultimately, neuronal death.[95] In contrast to neuronal loss, which is irreversible, disease-associated synaptic dysfunctions could be rescued through the growth of new terminals and/or dendritic spines.[5] Thus, focusing on early, prodromal dysfunction in PD appears key to design effective therapeutic and preventive strategies, and our study uncovered LRRK2 as a promising disease modifying target of early-stage PD.

Materials and methods

Mouse strains

C57Bl/6J Lrrk2 knock-out (KO) and G2019S-Lrrk2 knock-in mice were provided by Dr. Heather Melrose (Mayo Clinics, Florida, USA). Housing and handling of mice were done in compliance with national guidelines. All animal procedures were approved by the Ethical Committee of the University of Padova and the Italian Ministry of Health (license 1041/2016-PR and 105/2019) and followed the guidelines approved by the Northwestern University Animal Care and Use Committee. Approximately equal numbers of males and females were used for every experiment.

Cell cultures

Generation of LRRK2 KO SH-SY5Y CRISPR/Cas9 edited monoclonal cell line.

The KO of LRRK2 was performed using CRISPR/Cas9-mediated genome editing technology following the protocol by Sharma *et al.*[96] Two sgRNAs were selected among those designed by the laboratory of Zhang F (https://www.genscript.com/gRNA-detail/120892/LRRK2-CRISPR-guide-RNA.html) and one was designed using the online platform Benchling

(https://www.benchling.com). All the gRNAs were synthetized by Sigma-Aldrich. The oligos pairs encoding the 20-nt guide sequence were annealed and ligated into the pSpCas9(BB)-2A-Puro (PX459) V2.0 vector (Addgene, Watertown, MA, US) and then amplified in chemically competent E. coli StbI3 cells (ThermoFisher ScientificTM). SH-SY5Y cells were transfected using Lipofectamine 2000 (Invitrogen) and subjected to puromycin selection. The selected cells were diluted to obtain monoclonal cell lines. Approximately one week after plating, the colonies were inspected for a clonal appearance and progressively expanded. Finally, the deletion of LRRK2 was verified in multiple lines by western blot analysis with LRRK2 specific antibody (Fig. S3).

SH-SY5Y cell line maintenance, differentiation and treatments

Human neuroblastoma-derived SH-SY5Y cells (naïve, LRRK2 KO, expressing GFP or GFP-LRRK2 wild type) were cultured in a mixture (1:1) of Dulbecco's Modified Eagle's Medium (DMEM, Biowest) and Ham's F-12 Nutrient Mixture (F12, Biowest), supplemented with 10% (v/v) Fetal Bovine Serum (FBS, Thermo Fisher Scientific) and 1% Penicillin/Streptomycin solution (PS, GIBCO Life Technologies).

To promote N-type (neuronal-like cells) cell differentiation, cells were plated in DMEM/F12 containing 1% PS, 1% FBS and 10µM of all-trans-retinoic acid (RA, Sigma-Aldrich). At regular intervals of 48 hours, RA was newly provided to the medium. Cells were differentiated for 6 days and then subjected to the treatments.

SH-SY5Y cells were starved for 5 hours in DMEM/F12 supplemented with 1% PS and then stimulated with 100ng/mL BDNF (50240-MNAS, Sino Biological) for different time periods (5, 15, 30 and 60 minutes) in serum-free medium. LRRK2 kinase activity was inhibited pre-treating cells with 0.5µM MLi-2 (ab254528, Abcam) for 90 minutes.

Primary mouse cortical neuron preparation, transfection and treatments

Primary cortical neurons from Lrrk2 WT and KO C57BL/6J mice were derived from postnatal mouse (P0) exploiting the Papain Dissociation System (Worthington Biochemical Corporation). Cortices were incubated in Papain solution (Papain and DNase solution in Earle's Balanced Salt Solution) for 40 minutes at 37°C. Subsequently, tissue was triturated and

centrifugated for 5 minutes at 200g. The supernatant was discarded and the pellet was resuspended in Stop solution [DNase solution and Trypsin inhibitor solution (15,5mg/mL) in Earle's Balanced Salt Solution]. For 10 minutes the tissue was allowed to precipitate and then the supernatant was pipetted drop-by-drop on 5mL of 10/10 solution (10 µg/mL Trypsin inhibitor and 10 µg/mL BSA in Earle's Balanced Salt Solution) and centrifugated for 10 minutes at 100g. The pellet was resuspended in Neurobasal A medium (GIBCO Life Technologies) supplemented with 2% B27 supplement (GIBCO Life Technologies), 0.5 mM L-glutamine (GIBCO Life Technologies), 100 units/mL penicillin, and 100 µg/mL streptomycin (GIBCO Life Technologies). Cells were diluted and counted in 0.4% Trypan blue. Neurons were plated at 1000-1500 cells/mm^2 onto 6-well plates or at 200 cells/mm^2 on 12mm glass coverslips in 24-well plates and maintained in culture for 14 days prior to the treatments. After 7 days, 50% of the Neurobasal medium was removed and replaced with fresh one.

At DIV14, Lrrk2 WT and KO mature neurons cultured in the 6-well plates for western blot analysis were treated with MLi-2 (0.5µM) for 90 minutes and with BDNF (100ng/mL) for 5, 30, 60 and 180 minutes in Neurobasal completed medium. At DIV4, Lrrk2 WT and KO primary neurons plated in 24-well plates were transfected with lipofectamine (Lipofectamine 2000, Invitrogen) in a 1:2 ratio with DNA (v/w). The transfection was carried in Opti-MEM (GIBCO Life Technologies) for 45 minutes. Transfected neurons were then maintained in culture for additional 9-10 days. At DIV14, neurons were treated for 24 hours with 100ng/mL BDNF to study the spinogenesis process.

Media composition for cortical neuron differentiation from hiPSC

Neuronal maintenance media (NMM): 1:1 mixture of N2 media (DMEM/F12 GlutaMax supplemented with 1X N2, 50 units/mg/ml Penicillin/Streptomycin solution, 1X MEM Non-Essential Amino Acids Solution (100X), 100µM 2-Mercaptoethanol (ThermoFisher Scientific), 1mM sodium pyruvate and 5 µg/ml insulin (Merck)) and B27 media (Neurobasal supplemented with 1X B27 and 2mM L-Glutamine (ThermoFisher Scientific).

Neuronal induction media (NIM): NMM media supplemented with 100nM LDN193189 (Sigma Aldrich) and 10µM SB431542 (Bio-Techne).

hiPSC cell culture, cortical neuron differentiation and treatments

Isogenic human induced-pluripotent stem cell lines (hiPSC) of WT and LRRK2 KO, made and kindly provided by Mark R Cookson's laboratory,[59] were cultured using E8 media (Thermo Fisher Scientific) in a 6-well plate coated with Cultrex. Cortical neuronal differentiation was carried out according to Shi, *et al.*[58] Briefly, upon reaching 100% confluency, media was changed to neuronal induction media (NIM) and is marked as 0 days *in vitro* (DIV0). Daily NIM media change was carried out till DIV12, upon which neuronal precursor cells (NPCs) are generated. On DIV12, NPCs were expanded via passage at 1:2 ratio, supplemented with neuronal maintenance media (NMM) media and 20 ng/ml FGF2 (Bio-Techne). Neurogenesis was initiated on DIV18 with the removal of FGF2 and the cells supplemented with NMM only changing every 2 days. At DIV25-30, neurons were cryopreserved in CryoStor CS10 solution (Stem Cell technologies).

For electrophysiological recordings and immunocytochemistry/immunofluorescence (ICC/IF), thawed neurons were plated on Cultrex coated 10mm coverslips at a density of 60k/cm^2. All cells were treated with 1 ug/ml Mitomycin C (Sigma-Aldrich) for 1 hour at 37°C, 48-72 hours after plating to remove any proliferating cells. Neurons were maintained in NMM until used for experiments. BDNF treatment was carried out with cells incubated with 50 ng/ml BDNF (Bio-Techne) for 24 hours prior to use in electrophysiological recordings and ICC/IF.

Electrophysiological recordings

Whole-cell patch-clamp recordings were performed on cortical neurons at DIV70-75 (mentioned as DIV70 from here on) in voltage clamp at Vh −70 mV and the membrane test function was used to determine intrinsic membrane properties ∼1 min after obtaining whole-cell configuration, as described previously.[97] Briefly, coverslip containing neurons were transferred to warner bath (RC-26G) and maintained at 35 ± 2 ^{o}C through constant perfusion using in-line heater and controller (Warner Instruments) with extra cellular solution (ECS) containing (in mM unless stated): 145 NaCl, 3 KCl, 2 $MgCl_2$, 2 $CaCl_2$, 10 glucose, 10 HEPES, pH 7.4, 310 mOsm. Tetrodotoxin (TTX 0.2μM), and picrotoxin (PTX 100μM), were added before use to block sodium and $GABA_A$ currents. Pipette resistance (Rp) of glass electrodes was 4–6 MΩ when filled with (in mM): 130 Csmethanesulfonate, 5 CsCl, 4 NaCl, 2 MgCl2, 5

EGTA, 10 HEPES, 5 QX-314, 0.5 GTP, 10 Na2-phosphocreatine, and 5 MgATP, 0.1 spermine, pH 7.2, 300 mOsm. Data was acquired by Multiclamp700B amplifier and digidata 1550B and signals were filtered at 2kHz, digitized at 10 kHz, and analyzed in Clampfit 10 (MolecularDevices). Tolerance for series resistance (Rs) was <35 MΩ and uncompensated; ΔRs tolerance cut-off was <20%. mEPSCs were analyzed using Clampfit10 (threshold 5pA); all events were checked by eye. Data are presented as mean ± s.e.m. where n is cells from a minimum of 3 separate cultures (culture N in brackets).

Cells and tissues lysis, SDS-PAGE and Western blotting analysis

Immortalized cells, neurons and mouse brain tissues were lysed for 30 minutes on ice in appropriate volume of cold RIPA lysis buffer (Cell Signaling Technologies) supplemented with protease inhibitor cocktail. Protein concentration was assessed by performing BCA assay (Thermo Fisher Scientific). Proteins were solubilized in sample buffer (200mM Tris-HCl pH 6.8, 8% SDS, 400mM DTT, 40% glycerol, q.s. Bromophenol Blue) and resolved by SDS-PAGE on 8% Tris polyacrylamide homemade gels in Tris-glycine-SDS running buffer for the AP-MS experiments, and on 4-20% polyacrylamide gels (GenScript® Express Plus PAGE) in Tris-MOPS-SDS running buffer (GenScript® Running Buffer Powder) for the other cases. Proteins were transferred on PVDF (polyvinylidene difluoride, Bio-Rad) membranes using a semi-dry transfer system (Trans-Blot® Turbo Transfer System, Bio-Rad). Non-specific binding sites were blocked incubating membranes with 5% non-fat dry milk diluted in 0.1% Tween-20 Tris-buffered saline (TBS-T) for 1 hour at room temperature under agitation. Membranes were subsequently incubated overnight at 4°C with primary antibodies in 5% non-fat dry milk in TBS-T or in 5% BSA in TBS-T. After three washes in TBS-T at room temperature, membranes were incubated for 1 hour at room temperature with horseradish peroxidase (HRP)-conjugated goat anti-mouse or anti-rabbit IgG. After three more washes in TBS-T, proteins were visualized using chemiluminescence (Immobilon ECL western HRP substrate, Millipore). Densitometric analysis was carried out using the Image J software. The antibodies used for western blotting are as follows: rabbit α-LRRK2 (MJFF2 c41-2, ab133474, Abcam, 1:300); rabbit α-phospho-Ser935 LRRK2 (ab133450, Abcam, 1:300); mouse α-phospho-Ser473-AKT (sc-293125, Santa Cruz Biotechnology, 1:500); rabbit α-AKT (9272S, Cell Signaling Technology, 1:1000); rabbit α-phospho [(Thr202/Tyr204, Thr185/Tyr187)-ERK1/2 (12-302, Millipore, 1:1500); rabbit α-ERK1/2 (4695, Cell Signaling Technology,

1:1000); mouse α-GAPDH (CSB-MA000195, 1:5000); mouse α-βIII tubulin (T8578, Sigma-Aldrich, 1:40000); mouse α-DREBRIN (MA1-20377, Thermo Fisher Scientific, 1:500); α-Flag M2-HRP (A8592, Sigma-Aldrich, 1:5000); α-mouse IgG-HRP (A9044, Sigma-Aldrich, 1:80000); α-rabbit IgG-HRP (A9169, Sigma-Aldrich, 1:16000).

Staining on brain tissues and mammalian cells

Immunocytochemistry and confocal microscopy

Mouse primary cortical neurons derived from Lrrk2 WT C57BL/6 and KO pups (P0) were fixed using 4% paraformaldehyde (PFA, Sigma-Aldrich) in PBS1X pH 7.4 for 20 minutes at room temperature and, after three washes in PBS1X, they were subjected to staining protocol. Cells were firstly permeabilized with 0.3% Triton-X in PBS1X for 5 minutes and then saturated in blocking buffer [1% Bovine serum Albumin (BSA) Fraction V, 0.1% Triton-X, 50mM Glycine, 2% goat serum in PBS1X] for 1 hour at room temperature in agitation. The primary and secondary antibodies incubation steps were carried out in working solution (20% blocking buffer in PBS1X) for 1 hour at room temperature. Both incubations were followed by three washes in working solution. Nuclei staining was performed in Hoechst 33258 (Invitrogen, 1:10000 dilution in PBS1X) for 5 minutes and followed by three rinses in PBS1X. After been cleaning in distilled water, coverslips were mounted on microscope slides with Mowiol® mounting medium. Immunofluorescence z-stack images were obtained on Zeiss LSM700 laser scanning confocal microscope exploiting a 63X oil immersion objective.

The antibodies used for immunocytochemistry are as follows: mouse α-PSD95 (ab2723, Abcam, 1:200), rabbit α-MAP2 (sc-20172, Santa Cruz, 1:200); mouse α-drebrin (MA1-20377, Thermo Fisher Scientific, 1:400); goat anti-mouse-Alexa Fluor 568 (A11004, Invitrogen), goat anti-mouse-Alexa Fluor (A11004, Invitrogen), goat anti-rabbit-Alexa Fluor 488 (A11034, Invitrogen), rabbit-Alexa Fluor 568 (A11036, Invitrogen), goat anti-rabbit-Alexa Fluor 405.

Immunostaining and Image Analysis of hiPCS-derived cortical neurons

For immunocytochemistry DIV70 cells on coverslips were fixed in 4% paraformaldehyde (PFA) for 10 minutes. Cells were then permeabilized and blocked using 0.4% Tween with 10% normal goat serum (NGS), in PBS for 1 hour. Primary antibodies were incubated overnight at 4°C in PBST plus 10% NGS. Cells were washed 3× with PBST before 1 hour incubation at room temperature with secondary antibodies (α-guinea pig Alexa-488, α-rabbit Alexa 568, α-chicken 647 along with DAPI) from Molecular probes and Jackson Laboratories). Primary antibodies were chicken anti-microtubule associated protein 2 (MAP2) (Antibodies A85363, dil. 1:1000), rabbit anti-homer 1 (Synaptic Systems 160003, dil. 1:500), and guinea pig anti-bassoon (Synaptic Systems 141004, dil. 1:500). Coverslips were slide mounted with FluorSave (Sigma-Aldrich) and all images were acquired on Leica confocal microscope as 0.45 µm z-stacks at 60× magnification (flattened with the max projection function for cluster analysis). Single 60× images were used for analyses. Excitation and acquisition parameters were constrained across all experimental paired (culture) acquisitions. All images were analyzed using IMARIS microscopy image analysis software (v10.0.0 Oxford Instruments). Data are presented as mean ± s.e.m.

Golgi-Cox staining

Animals were terminally anesthetized and transcardially perfused with 0.9% saline. Half of each brain was incubated with Golgi-Cox solution (Potassium dichromate, Mercuric chloride, Potassium chromate prepared according to Zaqout *et al.*)[98] in the dark at room temperature for 14 days and then transferred in 30% sucrose solution in PBS1X. Brains were cut with a vibratome in 100 µm thick slices. The sections were then blotted by pressing an absorbent paper moistened with sucrose solution onto the slides and dried for 7-10 minutes. The samples were then subjected to color development procedure consisting in the following steps: 1. two 5-minutes washes in distilled water; 2. 5-minutes dehydration step in 50% ethanol; 3. 10-minutes incubation step in 20% ammonium hydroxide; 4. 5-minutes wash in distilled H_2O; 5. 8-minutes incubation step in 5% sodium thiosulfate at room temperature in the dark; 6. two additional 1-minute rinses in distilled H_2O; 7. dehydration in ascending grades of ethanol (70%, 95% and 100%). After two final 6-minutes incubations with xylene, the slides were covered with Eukitt® mounting medium. Images were acquired with Zeiss LSM700 laser scanning confocal microscope using 100X/1,40 Oil DIC M27 immersion objective with phase contrast acquisition

mode. All images were analyzed using freely available RECONSTRUCT software and according to Risher *et al*.[99]

Quantitative PCR

Total RNA was isolated from midbrain, striatum, and cortex of 1 month-old animals (n=6 animals per group, Lrrk2 WT and Lrrk2 KO) using Animal Tissue RNA Purification Kit (Norgen), according to manufacturer's instruction. After extraction, RNA concentration was quantified with NanoDrop 2000C spectrophotometer (Thermo Fisher Scientific). After DNAse treatment (Thermo Fisher Scientific, according to manufacturer's protocol), complementary DNA (cDNA) was generated using qRT SuperMix (Bimake). The cDNAs were used for quantitative PCR (qPCR) exploiting iTaq Universal SYBR® Green Supermix and CFX96 RealTime System (BioRad) for 40 cycles. All samples were triplicated, and transcripts levels normalized for RPL27 relative abundance (housekeeping gene). Data shown were produced using Bio-Rad CFX Manager software and analyzed according to ddCt algorithm. Primers (5'-3') used are: *Bdnf* FW: GGCTGACACTTTTGAGCACGTC and *Bdnf* REV: CTCCAAAGGCACTTGACTGCTG; *TrkB* FW: TGAGGAGGACACAGGATGTTGA and *Trkb* REV: TTCCAGTGCAAGCCAGTATCTG; *Shank3* FW: ACCTTGAGTCTGTAGATGTGGAAG and *Shank3* REV: GCTTGTGTCCAACCTTCACGAC; *Psd95* FW: GGTGACGACCCATCCATCTTTATC and *Psd95* REV: CGGACATCCACTTCATTGACAAAC; housekeeping *Rpl27* FW AAGCCGTCATCGTGAAGAACA and *Rpl27* REV: CTTGATCTTGGATCGCTTGGC.

Protein purification from mammalian cells

For the affinity purification (AP) protocol, SH-SY5Y GFP and SH-SY5Y GFP-LRRK2 cells were plated onto 100mm dishes and differentiated for 6 days. SH-SY5Y GFP-LRRK2 cells were treated with BDNF (100ng/mL) or with an equal volume of vehicle for 15 minutes, while SH-SY5Y OE-GFP cells were left untreated. Cells were harvested in lysis buffer (20mM Tris-HCl pH 7.5, 150mM NaCl, 1mM EDTA, 1% Tween 20, 2.5mM sodium pyrophosphate, 1mM β-glycerophosphate, 1mM sodium orthovanadate) supplemented with protease inhibitor cocktail (Sigma-Aldrich). Lysates were incubated end-over-end with GFP-TrapA beads (ChromoTek) overnight at 4°C. Immunocomplexes were subsequently washed ten times with

buffers containing a decreasing amount of NaCl and Tween20 and incubated with sample buffer 2X. The eluted proteins were resolved by SDS-PAGE and processed for Western Blot analysis or Mass Spectrometry (MS).

LC-MS/MS and data analysis

Three biological replicates of GFP-trap purifications of SH-SY5Y cells were processed for the proteomics experiments. Gels were stained with Colloidal Coomassie Brilliant Blue (0.25% Brilliant Blue R-250, 40% ethanol, 10% acetic acid in milli-Q water) for at least 1 hour and then rinsed in destaining solution (10% isopropanol, 10% acetic acid in milli-Q water). Gel slices were cut into small pieces and subjected to reduction with dithiothreitol (DTT 10 mM in 50 mM NH4HCO3, for 1 h at 56 °C), alkylation with iodoacetamide (55 mM in 50 mM NH4HCO3, for 45 min at RT and in the dark), and in-gel digestion with sequencing grade modified trypsin (Promega, 12.5 ng/µL in 50 mM NH4HCO3). Samples were analyzed with a LTQ-Orbitrap XL mass spectrometer (Thermo Fisher Scientific) coupled to a HPLC UltiMate 3000 (Dionex – Thermo Fisher Scientific) through a nanospray interface. Peptides were separated at a flow rate of 250 nL/min using an 11-cm-long capillary column (PicoFrit, 75-µm ID, 15-µm tip, New Objective) packed in house with C18 material (Aeris Peptide 3.6 µm XB C18; Phenomenex). A linear gradient of acetonitrile/0.1% formic acid from 3 to 40% was used for peptide separation and the instrument operated in a data dependent acquisition mode with a Top4 method (one full MS scan at 60,000 resolution in the Orbitrap, followed by the acquisition in the linear ion trap of the MS/MS spectra of the four most intense ions). Two technical replicates were acquired for each biological replicate. Raw data files were analyzed using MaxQuant and Andromeda software package[100] and searched against the human section of the UniProt database (version September 2020, 75093 entries) concatenated with a database of common contaminants found in proteomic experiments. Trypsin was selected as digesting enzyme with up to two missed cleavages allowed, carbamidomethylation of cysteine residues was set as a fixed modification and methionine oxidation as a variable modification. A search against a randomized database was used to assess the false discovery rate (FDR), and data were filtered to remove contaminants and reverse sequences and keep into account only proteins identified with at least two peptides and a FDR ≤ 0.01, both at peptide and protein level.

Intensity values were retrieved for 350 proteins. A single step of data QC was applied to the intensity values: proteins whose intensity value was 0.00 for both the 2 technical replicates in

at least 1 of the 3 pull-down experiments performed with LRRK2-GFP were removed. This is a stringent QC step, but it was implemented to remove proteins with no triplicate data available for the LRRK2 pull-down as this could have occurred because of genuine low levels of pull-down (values close to the limit of detection, missing not at random values) or because of technical issues with the single sample (loss/poor quality of sample, missing at random values). QC reduced the number of proteins in the analysis from 350 to 269 entries.

Intensity data were then processed according to Aguilan *et al.*[101] Briefly, intensity data were log2 transformed and normalized to the median of all proteins within the same experiment. Missing data (0.00 intensity values) were considered missing not at random thus they were imputed via probabilistic minimum imputation (random values within less than 2.5 standard deviations from the distribution of intensity values per the single experiment, 0.3 max variability).[101,102]

Finally, fold change (GFP-LRRK2 vs GFP and GFP-LRRK2 BDNF treated vs GFP-LRRK2 untreated) and associated p-value (two-tailed, paired t-test) were calculated and visualized.

Phosphoproteomics analysis

Protein processing for MS

Striata from 8 weeks mice were dissected and rapidly homogenized in four volumes of ice-cold Buffer A (0.32 M sucrose, 5 mM HEPES, pH7.4, 1 mM MgCl2, 0.5 mM CaCl2) supplemented with Halt protease and phosphatase inhibitor cocktail (Thermo Fisher Scientific) using a Teflon homogenizer (12 strokes). Homogenized brain extract was centrifuged at 1400g for 10 minutes. Supernatant (S1) was saved and pellet (P1) was homogenized in buffer A with a Teflon homogenizer (five strokes). After centrifugation at 700 g for 10 minutes, the supernatant (S1') was pooled with S1. Pooled S1 and S1′ were centrifuged at 13,800 g for 10 minutes to the crude synaptosomal pellet (P2). The crude synaptosomal pellet (P2) was homogenized in buffer B (0.32M sucrose, 6mM Tris, pH 8.0) supplemented with protease and phosphatase inhibitors cocktail with a Teflon homogenizer (five strokes) and was carefully loaded onto a discontinuous sucrose gradient (0.8 M/1 M/1.2 M sucrose solution in 6 mM Tris, pH 8.0) with a Pasteur pippete, followed by centrifugation in a swinging bucket rotor for 2 hours at 82,500g. The synaptic plasma membrane fraction (SPM) in the interphase between 1 M and 1.2 M sucrose fractions was collected using a syringe and transferred to clean ultracentrifuge tubes.

6 mM Tris buffer was added to each sample to adjust the sucrose concentration from 1.2 M to 0.32 M and the samples were centrifuged in a swinging bucket rotor at 200,000g for 30 minutes. The supernatant was removed and discarded. Added to the pellets the lysis solution containing 12 mM sodium deoxycholate, 12 mM sodium lauroyl sarcosinate, 10 mM TCEP, 40 mM CAA, and phosphatase inhibitor cocktail (Millipore-Sigma) in 50 mM Tris·HCl, pH 8.5, and incubated 10 min at 95°C with vigorous shaking. Sonicated the pellets several times with a sonicator probe and boiled again for 5 minutes. Centrifuged at 16,000g for 10 minutes to remove the debris and collected supernatant. The samples were diluted fivefold with 50 mM triethylammonium bicarbonate and analyzed by BCA to determine protein concentration. The samples were then normalized to 300µg protein in each and digested with 6µg Lys-C (Wako) for 3 hours at 37°C. 6µg trypsin was added for overnight digestion at 37°C. The supernatants were collected and acidified with trifluoroacetic acid (TFA) to a final concentration of 1% TFA. Ethyl acetate solution was added at 1:1 ratio to the samples. The mixture was vortexed for 2 minutes and then centrifuged at 16,000g for 2 minutes to obtain aqueous and organic phases. The organic phase (top layer) was removed, and the aqueous phase was collected, dried completely in a vacuum centrifuge, and desalted using Top-Tip C18 tips (Glygen) according to manufacturer's instructions. The samples were dried completely in a vacuum centrifuge and subjected to phosphopeptide enrichment using PolyMAC Phosphopeptide Enrichment kit (Tymora Analytical) according to manufacturer's instructions, and the eluted phosphopeptides dried completely in a vacuum centrifuge.

LC-MS/MS Analysis

The full phosphopeptide sample was dissolved in 10.5 µL of 0.05% trifluoroacetic acid with 3% (vol/vol) acetonitrile and 10 µL of each sample was injected into an Ultimate 3000 nano UHPLC system (Thermo Fisher Scientific). Peptides were captured on a 2-cm Acclaim PepMap trap column and separated on a 50-cm column packed with ReproSil Saphir 1.8 µm C18 beads (Dr. Maisch GmbH). The mobile phase buffer consisted of 0.1% formic acid in ultrapure water (buffer A) with an eluting buffer of 0.1% formic acid in 80% (vol/vol) acetonitrile (buffer B) run with a linear 90-min gradient of 6–30% buffer B at flow rate of 300 nL/min. The UHPLC was coupled online with a Q-Exactive HF-X mass spectrometer (Thermo Fisher Scientific). The mass spectrometer was operated in the data-dependent mode, in which a full-scan MS (from m/z 375 to 1,500 with the resolution of 60,000) was followed by MS/MS

of the 15 most intense ions (30,000 resolution; normalized collision energy - 28%; automatic gain control target (AGC) - 2E4, maximum injection time - 200 ms; 60sec exclusion].

LC-MS Data Processing

The raw files were searched directly against the mouse database with no redundant entries, using Byonic (Protein Metrics) and Sequest search engines loaded into Proteome Discoverer 2.3 software (Thermo Fisher Scientific). MS1 precursor mass tolerance was set at 10 ppm, and MS2 tolerance was set at 20ppm. Search criteria included a static carbamidomethylation of cysteines (+57.0214 Da), and variable modifications of phosphorylation of S, T and Y residues (+79.996 Da), oxidation (+15.9949 Da) on methionine residues and acetylation (+42.011 Da) at N terminus of proteins. Search was performed with full trypsin/P digestion and allowed a maximum of two missed cleavages on the peptides analyzed from the sequence database. The false-discovery rates of proteins and peptides were set at 0.01. All protein and peptide identifications were grouped and any redundant entries were removed. Only unique peptides and unique master proteins were reported.

Label-free Quantitation Analysis

All data were quantified using the label-free quantitation node of Precursor Ions Quantifier through the Proteome Discoverer v2.3 (Thermo Fisher Scientific). For the quantification of phosphoproteomic data, the intensities of phosphopeptides were extracted with initial precursor mass tolerance set at 10 ppm, minimum number of isotope peaks as 2, maximum ΔRT of isotope pattern multiplets – 0.2 min, PSM confidence FDR of 0.01, with hypothesis test of ANOVA, maximum RT shift of 5 min, pairwise ratio-based ratio calculation, and 100 as the maximum allowed fold change. For calculations of fold-change between the groups of proteins, total phosphoprotein abundance values were added together, and the ratios of these sums were used to compare proteins within different samples.

Bioinformatics

The LRRK2 interactome was constructed following the procedure reported in Zhao *et al.*[103] Briefly, protein interactions reported for LRRK2 in peer-reviewed literature were considered if the interaction was replicated in at least 2 different papers or identified with 2 different interaction detection methods. The obtained LRRK2 protein interaction network was analysed in Zhao *et al.*[44] to identify topological clusters using the FastGreed R Package (based on degree centrality). Here we report one of the identified clusters that is enriched for synaptic functions. Functional enrichment was performed using g:Profiler, g:GOSt (https://biit.cs.ut.ee/gprofiler/gost)[104] with Gene Ontology Biological Processes (GO-BPs) and SynGO (https://www.syngoportal.org/).

Statistical analysis

Statistical analyses and plotting were performed with GraphPad-Prism9. Unpaired, two-tailed t-test or Shapiro-Wilk test were used for experiments comparing two groups; one-way ANOVA was used for experiments comparing three or more groups; two-way ANOVA was used when multiple groups and two factors (i.e., genotype and treatment) were to be compared. Šídák's multiple comparisons test was used when determining statistical significance for comparisons between groups.

Data availability

The authors confirm that the data supporting the findings of this study are available within the article and its supplementary material.

Protein composition of the LRRK2 cluster enriched for synaptic functions can be obtained from Zhao *et al.*[103]

Funding

This work was supported by the University of Padova [STARS Grants, LRRKing-Role of the Parkinson's disease kinase LRRK2 in shaping neurites and synapses, EG), the Michael J. Fox Foundation for Parkinson's Research-LRRK2 challenge (EG, LP and CM), NIH R01 NS097901 (LP), UKRI future Leader Fellowship funding MR/T041129/1 (DBK).

Acknowledgments

We are very grateful to Dr. Mark R Cookson and Alexandra Beilina (NIA, NIH, USA) for providing WT and LRRK2 KO human iPSC lines used for electrophysiological measurements.

Competing interests

The authors report no competing interests.

References

1. Fiala JC, Spacek J, Harris KM. Dendritic spine pathology: Cause or consequence of neurological disorders? *Brain Res Rev*. 2002;39(1):29-54. doi:10.1016/S0165-0173(02)00158-3

2. Hong S, Beja-Glasser VF, Nfonoyim BM, et al. Complement and microglia mediate early synapse loss in Alzheimer mouse models. *Science (1979)*. 2016;352(6286):712-716. doi:10.1126/science.aad8373

3. Milnerwood AJ, Raymond LA. Early synaptic pathophysiology in neurodegeneration: Insights from Huntington's disease. *Trends Neurosci*. 2010;33(11):513-523. doi:10.1016/j.tins.2010.08.002

4. Soukup S, Vanhauwaert R, Verstreken P. Parkinson's disease: convergence on synaptic homeostasis. *EMBO J*. 2018;37(18). doi:10.15252/embj.201898960

5. Picconi B, Piccoli G, Calabresi P. Synaptic dysfunction in Parkinson's disease. *Adv Exp Med Biol*. 2012;970:553-572. doi:10.1007/978-3-7091-0932-8_24/FIGURES/1

6. Kordower JH, Olanow CW, Dodiya HB, et al. Disease duration and the integrity of the nigrostriatal system in Parkinson's disease. *Brain*. 2013;136(8):2419-2431. doi:10.1093/brain/awt192

7. Bellucci A, Antonini A, Pizzi M, Spano PF. The end is the beginning: Parkinson's disease in the light of brain imaging. *Front Aging Neurosci*. 2017;9(OCT). doi:10.3389/fnagi.2017.00330

8. Chidambaram SB, Rathipriya AG, Bolla SR, et al. Dendritic spines: Revisiting the physiological role. *Prog Neuropsychopharmacol Biol Psychiatry*. 2019;92:161-193. doi:10.1016/j.pnpbp.2019.01.005

9. González-Rodríguez P, Zampese E, Stout KA, et al. Disruption of mitochondrial complex I induces progressive parkinsonism. *Nature*. 2021;599(7886):650-656. doi:10.1038/s41586-021-04059-0

10. Cookson MR. LRRK2 Pathways Leading to Neurodegeneration. *Curr Neurol Neurosci Rep*. 2015;15(7). doi:10.1007/s11910-015-0564-y

11. Greggio E, Cookson MR. Leucine-rich repeat kinase 2 mutations and Parkinson's disease: Three questions. *ASN Neuro*. 2009;1(1):13-24. doi:10.1042/AN20090007

12. Marchand A, Drouyer M, Sarchione A, Chartier-Harlin MC, Taymans JM. LRRK2 Phosphorylation, More Than an Epiphenomenon. *Front Neurosci*. 2020;14. doi:10.3389/fnins.2020.00527

13. Wallings R, Manzoni C, Bandopadhyay R. Cellular processes associated with LRRK2 function and dysfunction. *FEBS Journal*. 2015;282(15):2806-2826. doi:10.1111/febs.13305

14. Civiero L, Cogo S, Biosa A, Greggio E. The role of LRRK2 in cytoskeletal dynamics. *Biochem Soc Trans*. 2018;46(6):1653-1663. doi:10.1042/BST20180469

15. Iannotta L, Greggio E. LRRK2 signaling in neurodegeneration: two decades of progress. Halliday G, Dzamko N, eds. *Essays Biochem*. 2021;65(7):859-872. doi:10.1042/ebc20210013

16. Nichols RJ, Dzamko N, Morrice NA, et al. 14-3-3 Binding to LRRK2 is disrupted by multiple Parkinson's disease-associated mutations and regulates cytoplasmic localization. *Biochemical Journal*. 2010;430(3):393-404. doi:10.1042/BJ20100483

17. Dzamko N, Inesta-Vaquera F, Zhang J, et al. The IkappaB kinase family phosphorylates the Parkinson's disease kinase LRRK2 at Ser935 and Ser910 during Toll-Like Receptor signaling. *PLoS One*. 2012;7(6). doi:10.1371/journal.pone.0039132

18. Muda K, Bertinetti D, Gesellchen F, et al. Parkinson-related LRRK2 mutation R1441C/G/H impairs PKA phosphorylation of LRRK2 and disrupts its interaction with 14-3-3. *Proc Natl Acad Sci U S A*. 2014;111(1). doi:10.1073/pnas.1312701111

19. Chia R, Haddock S, Beilina A, et al. Phosphorylation of LRRK2 by casein kinase 1α regulates trans-Golgi clustering via differential interaction with ARHGEF7. *Nat Commun*. 2014;5. doi:10.1038/ncomms6827

20. Dzamko N, Deak M, Hentati F, et al. Inhibition of LRRK2 kinase activity leads to dephosphorylation of Ser 910/Ser935, disruption of 14-3-3 binding and altered cytoplasmic localization. *Biochemical Journal*. 2010;430(3):405-413. doi:10.1042/BJ20100784

21. Nazish I, Arber C, Piers TM, et al. Abrogation of LRRK2 dependent Rab10 phosphorylation with TLR4 activation and alterations in evoked cytokine release in immune cells. *Neurochem Int*. 2021;147. doi:10.1016/j.neuint.2021.105070

22. Pischedda F, Piccoli G. LRRK2 at the pre-synaptic site: A 16-years perspective. *J Neurochem*. 2021;157(2):297-311. doi:10.1111/jnc.15240

23. Belluzzi E, Gonnelli A, Cirnaru MD, et al. LRRK2 phosphorylates pre-synaptic N-ethylmaleimide sensitive fusion (NSF) protein enhancing its ATPase activity and SNARE complex disassembling rate. *Mol Neurodegener*. 2016;11(1):1-16. doi:10.1186/S13024-015-0066-Z/FIGURES/6

24. Marte A, Russo I, Rebosio C, et al. Leucine-rich repeat kinase 2 phosphorylation on synapsin I regulates glutamate release at pre-synaptic sites. *J Neurochem*. 2019;150(3):264-281. doi:10.1111/jnc.14778

25. Soukup SF, Kuenen S, Vanhauwaert R, et al. A LRRK2-Dependent EndophilinA Phosphoswitch Is Critical for Macroautophagy at Presynaptic Terminals. *Neuron*. 2016;92(4):829-844. doi:10.1016/J.NEURON.2016.09.037

26. Cao M, Wu Y, Ashrafi G, et al. Parkinson Sac Domain Mutation in Synaptojanin 1 Impairs Clathrin Uncoating at Synapses and Triggers Dystrophic Changes in Dopaminergic Axons. *Neuron*. 2017;93(4):882-896.e5. doi:10.1016/J.NEURON.2017.01.019

27. Nguyen M, Krainc D. LRRK2 phosphorylation of auxilin mediates synaptic defects in dopaminergic neurons from patients with Parkinson's disease. *Proc Natl Acad Sci U S A*. 2018;115(21):5576-5581. doi:10.1073/PNAS.1717590115/SUPPL_FILE/PNAS.1717590115.SD02.XLSX

28. Rassu M, Del Giudice MG, Sanna S, et al. Role of LRRK2 in the regulation of dopamine receptor trafficking. *PLoS One*. 2017;12(6). doi:10.1371/journal.pone.0179082

29. Chen C, Soto G, Dumrongprechachan V, et al. Pathway-specific dysregulation of striatal excitatory synapses by LRRK2 mutations. *Elife*. 2020;9:1-26. doi:10.7554/eLife.58997

30. Matikainen-Ankney BA, Kezunovic N, Mesias RE, et al. Altered development of synapse structure and function in striatum caused by Parkinson's disease-linked LRRK2-G2019S mutation. *Journal of Neuroscience*. 2016;36(27):7128-7141. doi:10.1523/JNEUROSCI.3314-15.2016

31. Parisiadou L, Yu J, Sgobio C, et al. LRRK2 regulates synaptogenesis and dopamine receptor activation through modulation of PKA activity. *Nat Neurosci*. 2014;17(3):367-376. doi:10.1038/NN.3636

32. Thoenen H. Neurotrophins and neuronal plasticity. *Science (1979)*. 1995;270(5236):593-598. doi:10.1126/science.270.5236.593

33. Baydyuk M, Xu B. BDNF signaling and survival of striatal neurons. *Front Cell Neurosci*. 2014;8(AUG). doi:10.3389/fncel.2014.00254

34. Iannotta L, Biosa A, Kluss JH, et al. Divergent Effects of G2019S and R1441C LRRK2 Mutations on LRRK2 and Rab10 Phosphorylations in Mouse Tissues. *Cells*. 2020;9(11). doi:10.3390/cells9112344

35. Skelton PD, Tokars V, Parisiadou L. LRRK2 at Striatal Synapses: Cell-Type Specificity and Mechanistic Insights. *Cells*. 2022;11(1). doi:10.3390/cells11010169

36. Piccoli G, Condliffe SB, Bauer M, et al. LRRK2 controls synaptic vesicle storage and mobilization within the recycling pool. *Journal of Neuroscience*. 2011;31(6):2225-2237. doi:10.1523/JNEUROSCI.3730-10.2011

37. Kluss JH, Lewis PA, Greggio E. Leucine-rich repeat kinase 2 (LRRK2): an update on the potential therapeutic target for Parkinson's disease. *Expert Opin Ther Targets*. 2022;26(6):537-546. doi:10.1080/14728222.2022.2082937

38. Encinas M, Iglesias M, Liu Y, et al. Sequential treatment of SH-SY5Y cells with retinoic acid and brain-derived neurotrophic factor gives rise to fully differentiated, neurotrophic factor-dependent, human neuron-like cells. *J Neurochem*. 2000;75(3):991-1003. doi:10.1046/j.1471-4159.2000.0750991.x

39. Numakawa T, Suzuki S, Kumamaru E, Adachi N, Richards M, Kunugi H. BDNF function and intracellular signaling in neurons. *Histol Histopathol*. 2010;25(2):237-258. doi:10.14670/HH-25.237

40. Manzoni C, Denny P, Lovering RC, Lewis PA. Computational analysis of the LRRK2 interactome. *PeerJ*. 2015;2015(2). doi:10.7717/peerj.778

41. Tomkins JE, Dihanich S, Beilina A, et al. Comparative Protein Interaction Network Analysis Identifies Shared and Distinct Functions for the Human ROCO Proteins. *Proteomics*. 2018;18(10). doi:10.1002/pmic.201700444

42. Koopmans F, van Nierop P, Andres-Alonso M, et al. SynGO: An Evidence-Based, Expert-Curated Knowledge Base for the Synapse. *Neuron*. 2019;103(2):217-234.e4. doi:10.1016/j.neuron.2019.05.002

43. Koganezawa N, Hanamura K, Sekino Y, Shirao T. The role of drebrin in dendritic spines. *Molecular and Cellular Neuroscience*. 2017;84:85-92. doi:10.1016/j.mcn.2017.01.004

44. Zhao Y, Harvey K, Escott-Price V, Lewis PA, Manzoni C. Transcriptomics analyses of the LRRK2 protein interactome reveal distinct molecular signatures for sporadic and

LRRK2 Parkinson's Disease. *bioRxiv*. Published online September 13, 2023:2023.09.12.557373. doi:10.1101/2023.09.12.557373

45. Spirin V, Mirny LA. Protein complexes and functional modules in molecular networks. *Proc Natl Acad Sci U S A*. 2003;100(21):12123-12128. doi:10.1073/PNAS.2032324100

46. Meixner A, Boldt K, Van Troys M, et al. A QUICK screen for Lrrk2 interaction partners--leucine-rich repeat kinase 2 is involved in actin cytoskeleton dynamics. *Mol Cell Proteomics*. 2011;10(1). doi:10.1074/MCP.M110.001172

47. Liu Z, Lee J, Krummey S, Lu W, Cai H, Lenardo MJ. The kinase LRRK2 is a regulator of the transcription factor NFAT that modulates the severity of inflammatory bowel disease. *Nature Immunology 2011 12:11*. 2011;12(11):1063-1070. doi:10.1038/ni.2113

48. Kellner Y, Gödecke N, Dierkes T, Thieme N, Zagrebelsky M, Korte M. The BDNF effects on dendritic spines of mature hippocampal neurons depend on neuronal activity. *Front Synaptic Neurosci*. 2014;6(MAR). doi:10.3389/fnsyn.2014.00005

49. Zagrebelsky M, Korte M. Form follows function: BDNF and its involvement in sculpting the function and structure of synapses. *Neuropharmacology*. 2014;76(PART C):628-638. doi:10.1016/j.neuropharm.2013.05.029

50. Lai KO, Wong ASL, Cheung MC, et al. TrkB phosphorylation by Cdk5 is required for activity-dependent structural plasticity and spatial memory. *Nat Neurosci*. 2012;15(11):1506-1515. doi:10.1038/nn.3237

51. Ji Y, Pang PT, Feng L, Lu B. Cyclic AMP controls BDNF-induced TrkB phosphorylation and dendritic spine formation in mature hippocampal neurons. *Nat Neurosci*. 2005;8(2):164-172. doi:10.1038/nn1381

52. Lendvai B, Stern EA, Chen B, Svoboda K. Experience-dependent plasticity of dendritic spines in the developing rat barrel cortex in vivo. *Nature 2000 404:6780*. 2000;404(6780):876-881. doi:10.1038/35009107

53. Koleske AJ. Molecular mechanisms of dendrite stability. *Nat Rev Neurosci*. 2013;14(8):536-550. doi:10.1038/nrn3486

54. Surmeier DJ, Obeso JA, Halliday GM. Selective neuronal vulnerability in Parkinson disease. *Nat Rev Neurosci*. 2017;18(2):101-113. doi:10.1038/nrn.2016.178

55. Westerlund M, Belin AC, Anvret A, Bickford P, Olson L, Galter D. Developmental regulation of leucine-rich repeat kinase 1 and 2 expression in the brain and other rodent and human organs: Implications for Parkinson's disease. *Neuroscience*. 2008;152(2):429-436. doi:10.1016/j.neuroscience.2007.10.062

56. Tong Y, Pisani A, Martella G, et al. R1441C mutation in LRRK2 impairs dopaminergic neurotransmission in mice. *Proc Natl Acad Sci U S A*. 2009;106(34):14622-14627. doi:10.1073/pnas.0906334106

57. Volta M, Beccano-Kelly DA, Paschall SA, et al. Initial elevations in glutamate and dopamine neurotransmission decline with age, as does exploratory behavior, in LRRK2 G2019S knock-in mice. *Elife*. 2017;6. doi:10.7554/ELIFE.28377

58. Shi Y, Kirwan P, Livesey FJ. Directed differentiation of human pluripotent stem cells to cerebral cortex neurons and neural networks. *Nature Protocols 2012 7:10*. 2012;7(10):1836-1846. doi:10.1038/nprot.2012.116

59. Beylina A, Langston RG, Rosen D, Reed X, Cookson MR. Generation of fourteen isogenic cell lines for Parkinson's disease-associated leucine-rich repeat kinase (LRRK2). *Stem Cell Res*. 2021;53:102354. doi:10.1016/J.SCR.2021.102354

60. Lee JH, Han JH, Kim H, Park SM, Joe EH, Jou I. Parkinson's disease-associated LRRK2-G2019S mutant acts through regulation of SERCA activity to control ER stress in astrocytes. *Acta Neuropathol Commun*. 2019;7(1):68. doi:10.1186/S40478-019-0716-4

61. Reyniers L, Del Giudice MG, Civiero L, et al. Differential protein protein interactions of LRRK1 and LRRK2 indicate roles in distinct cellular signaling pathways. *J Neurochem*. 2014;131(2):239-250. doi:10.1111/jnc.12798

62. Dächsel JC, Taylor JP, Mok SS, et al. Identification of potential protein interactors of Lrrk2. *Parkinsonism Relat Disord*. 2007;13(7):382-385. doi:10.1016/j.parkreldis.2007.01.008

63. Liu GH, Qu J, Suzuki K, et al. Progressive degeneration of human neural stem cells caused by pathogenic LRRK2. *Nature*. 2012;491(7425):603-607. doi:10.1038/nature11557

64. Worth DC, Daly CN, Geraldo S, Oozeer F, Gordon-Weeks PR. Drebrin contains a cryptic F-actin–bundling activity regulated by Cdk5 phosphorylation. *Journal of Cell Biology*. 2013;202(5):793-806. doi:10.1083/JCB.201303005

65. Blom N, Gammeltoft S, Brunak S. Sequence and structure-based prediction of eukaryotic protein phosphorylation sites. *J Mol Biol*. 1999;294(5):1351-1362. doi:10.1006/jmbi.1999.3310

66. Blom N, Sicheritz-Pontén T, Gupta R, Gammeltoft S, Brunak S. Prediction of post-translational glycosylation and phosphorylation of proteins from the amino acid sequence. *Proteomics*. 2004;4(6):1633-1649. doi:10.1002/pmic.200300771

67. Beccano-Kelly DA, Kuhlmann N, Tatarnikov I, et al. Synaptic function is modulated by LRRK2 and glutamate release is increased in cortical neurons of G2019S LRRK2 knock-in mice. *Front Cell Neurosci*. 2014;8(SEP):1-11. doi:10.3389/FNCEL.2014.00301/BIBTEX

68. Beccano-Kelly DA, Volta M, Lise LN, et al. LRRK2 overexpression alters glutamatergic presynaptic plasticity, striatal dopamine tone, postsynaptic signal transduction, motor activity and memory. *Hum Mol Genet*. 2015;24(5):1336-1349. doi:10.1093/HMG/DDU543

69. Piccoli G, Onofri F, Cirnaru MD, et al. Leucine-Rich Repeat Kinase 2 Binds to Neuronal Vesicles through Protein Interactions Mediated by Its C-Terminal WD40 Domain. *Mol Cell Biol*. 2014;34(12):2147-2161. doi:10.1128/mcb.00914-13

70. Cirnaru MD, Marte A, Belluzzi E, et al. LRRK2 kinase activity regulates synaptic vesicle trafficking and neurotransmitter release through modulation of LRRK2 macro-molecular complex. *Front Mol Neurosci*. 2014;7(MAY). doi:10.3389/fnmol.2014.00049

71. Maas JW, Yang J, Edwards RH. Endogenous leucine-rich repeat kinase 2 slows synaptic vesicle recycling in striatal neurons. *Front Synaptic Neurosci*. 2017;9(FEB). doi:10.3389/fnsyn.2017.00005

72. Arranz AM, Delbroek L, van Kolen K, et al. LRRK2 functions in synaptic vesicle endocytosis through a kinasedependent mechanism. *J Cell Sci*. 2015;128(3):541-552. doi:10.1242/jcs.158196

73. Hedrick NG, Harward SC, Hall CE, Murakoshi H, McNamara JO, Yasuda R. Rho GTPase complementation underlies BDNF-dependent homo- and heterosynaptic plasticity. *Nature*. 2016;538(7623):104-108. doi:10.1038/nature19784

74. Chan D, Citro A, Cordy JM, Shen GC, Wolozin B. Rac1 protein rescues neurite retraction caused by G2019s leucine-rich repeat kinase 2 (LRRK2). *Journal of Biological Chemistry*. 2011;286(18):16140-16149. doi:10.1074/jbc.M111.234005

75. Feng M, Hu X, Li N, et al. Distinctive roles of Rac1 and Rab29 in LRRK2 mediated membrane trafficking and neurite outgrowth. *J Biomed Res*. 2018;32(2):145-156. doi:10.7555/JBR.31.20170039

76. Takahashi H, Sekino Y, Tanaka S, Mizui T, Kishi S, Shirao T. Drebrin-dependent actin clustering in dendritic filopodia governs synaptic targeting of postsynaptic density-95 and dendritic spine morphogenesis. *Journal of Neuroscience*. 2003;23(16):6586-6595. doi:10.1523/jneurosci.23-16-06586.2003

77. Aoki C, Kojima N, Sabaliauskas N, et al. Drebrin a knockout eliminates the rapid form of homeostatic synaptic plasticity at excitatory synapses of intact adult cerebral cortex. *Journal of Comparative Neurology*. 2009;517(1):105-121. doi:10.1002/cne.22137

78. Sekino Y, Tanaka S, Hanamura K, et al. Activation of N-methyl-d-aspartate receptor induces a shift of drebrin distribution: Disappearance from dendritic spines and appearance in dendritic shafts. *Molecular and Cellular Neuroscience*. 2006;31(3):493-504. doi:10.1016/j.mcn.2005.11.003

79. Spence EF, Kanak DJ, Carlson BR, Soderling SH. The Arp2/3 complex is essential for distinct stages of spine synapse maturation, including synapse unsilencing. *Journal of Neuroscience*. 2016;36(37):9696-9709. doi:10.1523/JNEUROSCI.0876-16.2016

80. Kim KS, Marcogliese PC, Yang J, et al. Regulation of myeloid cell phagocytosis by LRRK2 via WAVE2 complex stabilization is altered in Parkinson's disease. *Proc Natl Acad Sci U S A*. 2018;115(22):E5164-E5173. doi:10.1073/pnas.1718946115

81. Giaime E, Tong Y, Wagner LK, Yuan Y, Huang G, Shen J. Age-Dependent Dopaminergic Neurodegeneration and Impairment of the Autophagy-Lysosomal Pathway in LRRK-Deficient Mice. *Neuron*. 2017;96(4):796-807.e6. doi:10.1016/j.neuron.2017.09.036

82. Huang G, Bloodgood DW, Kang J, et al. Motor Impairments and Dopaminergic Defects Caused by Loss of Leucine-Rich Repeat Kinase Function in Mice. *J Neurosci*. 2022;42(23):4755-4765. doi:10.1523/JNEUROSCI.0140-22.2022

83. Biskup S, Moore DJ, Rea A, et al. Dynamic and redundant regulation of LRRK2 and LRRK1 expression. *BMC Neurosci*. 2007;8. doi:10.1186/1471-2202-8-102

84. Cogo S, Ho FY, Tosoni E, et al. The Roc domain of LRRK2 as a hub for protein-protein interactions: a focus on PAK6 and its impact on RAB phosphorylation. *Brain Res*. 2022;1778. doi:10.1016/j.brainres.2022.147781

85. Qualmann B, Boeckers TM, Jeromin M, Gundelfinger ED, Kessels MM. Linkage of the Actin Cytoskeleton to the Postsynaptic Density via Direct Interactions of Abp1 with the ProSAP/Shank Family. *Journal of Neuroscience*. 2004;24(10):2481-2495. doi:10.1523/JNEUROSCI.5479-03.2004

86. Narita M, Aoki K, Takagi M, Yajima Y, Suzuki T. Implication of brain-derived neurotrophic factor in the release of dopamine and dopamine-related behaviors induced by methamphetamine. *Neuroscience*. 2003;119(3):767-775. doi:10.1016/S0306-4522(03)00099-X

87. Morella I, Hallum H, Brambilla R. Dopamine D1 and Glutamate Receptors Co-operate With Brain-Derived Neurotrophic Factor (BDNF) and TrkB to Modulate ERK Signaling in Adult Striatal Slices. *Front Cell Neurosci*. 2020;14. doi:10.3389/fncel.2020.564106

88. Hyman C, Hofer M, Barde YA, et al. BDNF is a neurotrophic factor for dopaminergic neurons of the substantia nigra. *Nature*. 1991;350(6315):230-232. doi:10.1038/350230a0

89. Baquet ZC, Bickford PC, Jones KR. Brain-derived neurotrophic factor is required for the establishment of the proper number of dopaminergic neurons in the substantia nigra pars compacta. *Journal of Neuroscience*. 2005;25(26):6251-6259. doi:10.1523/JNEUROSCI.4601-04.2005

90. Rahmani F, Saghazadeh A, Rahmani M, et al. Plasma levels of brain-derived neurotrophic factor in patients with Parkinson disease: A systematic review and meta-analysis. *Brain Res*. 2019;1704:127-136. doi:10.1016/j.brainres.2018.10.006

91. Lin CH, Wu RM, Tai CH, Chen ML, Hu FC. Lrrk2 S1647T and BDNF V66M interact with environmental factors to increase risk of Parkinson's disease. *Parkinsonism Relat Disord*. 2011;17(2):84-88. doi:10.1016/j.parkreldis.2010.11.011

92. Liu J, Zhou Y, Wang C, Wang T, Zheng Z, Chan P. Brain-derived neurotrophic factor (BDNF) genetic polymorphism greatly increases risk of leucine-rich repeat kinase 2 (LRRK2) for Parkinson's disease. *Parkinsonism Relat Disord*. 2012;18(2):140-143. doi:10.1016/j.parkreldis.2011.09.002

93. Siuda J, Patalong-Ogiewa M, Żmuda W, et al. Cognitive impairment and BDNF serum levels. *Neurol Neurochir Pol*. 2017;51(1):24-32. doi:10.1016/j.pjnns.2016.10.001

94. Ziebell M, Khalid U, Klein AB, et al. Striatal dopamine transporter binding correlates with serum BDNF levels in patients with striatal dopaminergic neurodegeneration. *Neurobiol Aging*. 2012;33(2):428.e1-428.e5. doi:10.1016/j.neurobiolaging.2010.11.010

95. Tagliaferro P, Burke RE. Retrograde Axonal Degeneration in Parkinson Disease. *J Parkinsons Dis*. 2016;6(1):1-15. doi:10.3233/JPD-150769

96. Sharma A, Toepfer CN, Ward T, et al. CRISPR/Cas9-Mediated Fluorescent Tagging of Endogenous Proteins in Human Pluripotent Stem Cells. *Curr Protoc Hum Genet*. 2018;96(1):21.11.1-21.11.20. doi:10.1002/CPHG.52

97. Beccano-Kelly DA, Cherubini M, Mousba Y, et al. Calcium dysregulation combined with mitochondrial failure and electrophysiological maturity converge in Parkinson's iPSC-dopamine neurons. *iScience*. 2023;26(7):107044. doi:10.1016/J.ISCI.2023.107044

98. Zaqout S, Kaindl AM. Golgi-cox staining step by step. *Front Neuroanat*. 2016;10:181342. doi:10.3389/FNANA.2016.00038/BIBTEX

99. Risher WC, Ustunkaya T, Alvarado JS, Eroglu C. Rapid Golgi Analysis Method for Efficient and Unbiased Classification of Dendritic Spines. *PLoS One*. 2014;9(9):e107591. doi:10.1371/JOURNAL.PONE.0107591

100. Tyanova S, Temu T, Cox J. The MaxQuant computational platform for mass spectrometry-based shotgun proteomics. *Nature Protocols 2016 11:12*. 2016;11(12):2301-2319. doi:10.1038/nprot.2016.136

101. Aguilan JT, Kulej K, Sidoli S. Guide for protein fold change and: P-value calculation for non-experts in proteomics. *Mol Omics*. 2020;16(6):573-582. doi:10.1039/d0mo00087f

102. Lazar C, Gatto L, Ferro M, Bruley C, Burger T. Accounting for the Multiple Natures of Missing Values in Label-Free Quantitative Proteomics Data Sets to Compare Imputation Strategies. *J Proteome Res*. 2016;15(4):1116-1125. doi:10.1021/acs.jproteome.5b00981

103. Zhao Y, Vavouraki N, Lovering RC, et al. Tissue specific LRRK2 interactomes reveal a distinct striatal functional unit. *PLoS Comput Biol*. 2023;19(1):e1010847. doi:10.1371/JOURNAL.PCBI.1010847

104. Raudvere U, Kolberg L, Kuzmin I, et al. g:Profiler: a web server for functional enrichment analysis and conversions of gene lists (2019 update). *Nucleic Acids Res*. 2019;47(W1):W191-W198. doi:10.1093/NAR/GKZ369

Figures

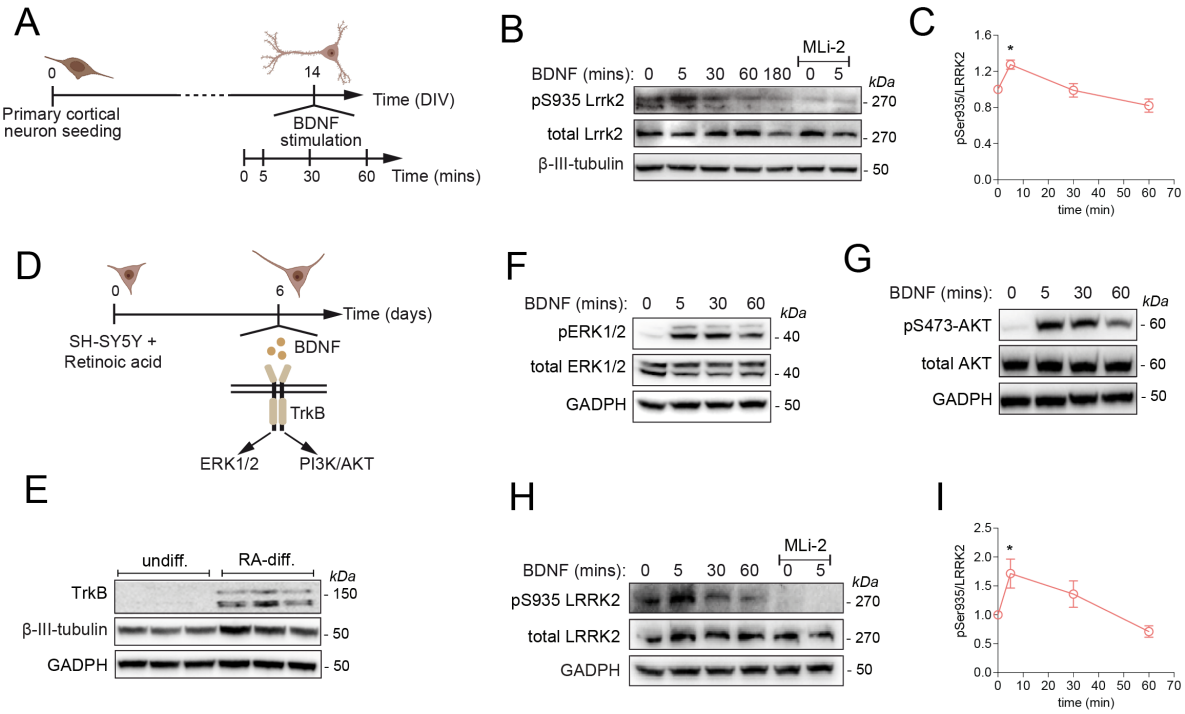

Figure 1. LRRK2 phosphorylation at ser935 rapidly and transiently increases upon BDNF stimulation in primary mouse cortical neurons and differentiated SH-SY5Y cells. **(A)** Schematic representation of the experimental setting of (B). **(B)** Phospho-Ser935 and total Lrrk2 protein levels of primary cortical neurons at DIV14 treated with 100 ng/mL BDNF for 0, 5, 30, 60 180 mins. MLi-2 was used at 500 nM for 90 mins to inhibit Lrrk2 kinase activity. **(C)** Quantification of n=6 independent experiments of (B). One-way ANOVA, Dunnett's multiple comparison test (*P < 0.05 t=0 vs. t=5'). **(D)** Schematic representation of the experimental setting of (F) and (G). **(E)** TrkB protein levels in undifferentiated or retinoic acid-differentiated SH-SY5Y cells. **(F)** Phospho Thr202/185 ERK1/2, total ERK1/2 and **(G)** phospho Ser473 AKT, total AKT protein levels of retinoic acid-differentiated SH-SY5Y cells stimulated with 100 ng/mL BDNF for 0, 5, 30, 60 mins. **(H)** Phospho-Ser935 and total Lrrk2 protein levels of retinoic acid-differentiated SH-SY5Y cells stimulated with 100 ng/mL BDNF for 0, 5, 30, 60 mins. MLi-2 was used at 500 nM for 90 mins to inhibit Lrrk2 kinase activity. **(I)** Quantification of (G) (n=4 independent experiments). One-way ANOVA, Dunnett's multiple comparison test (*P < 0.05 t=0 vs. t=5').

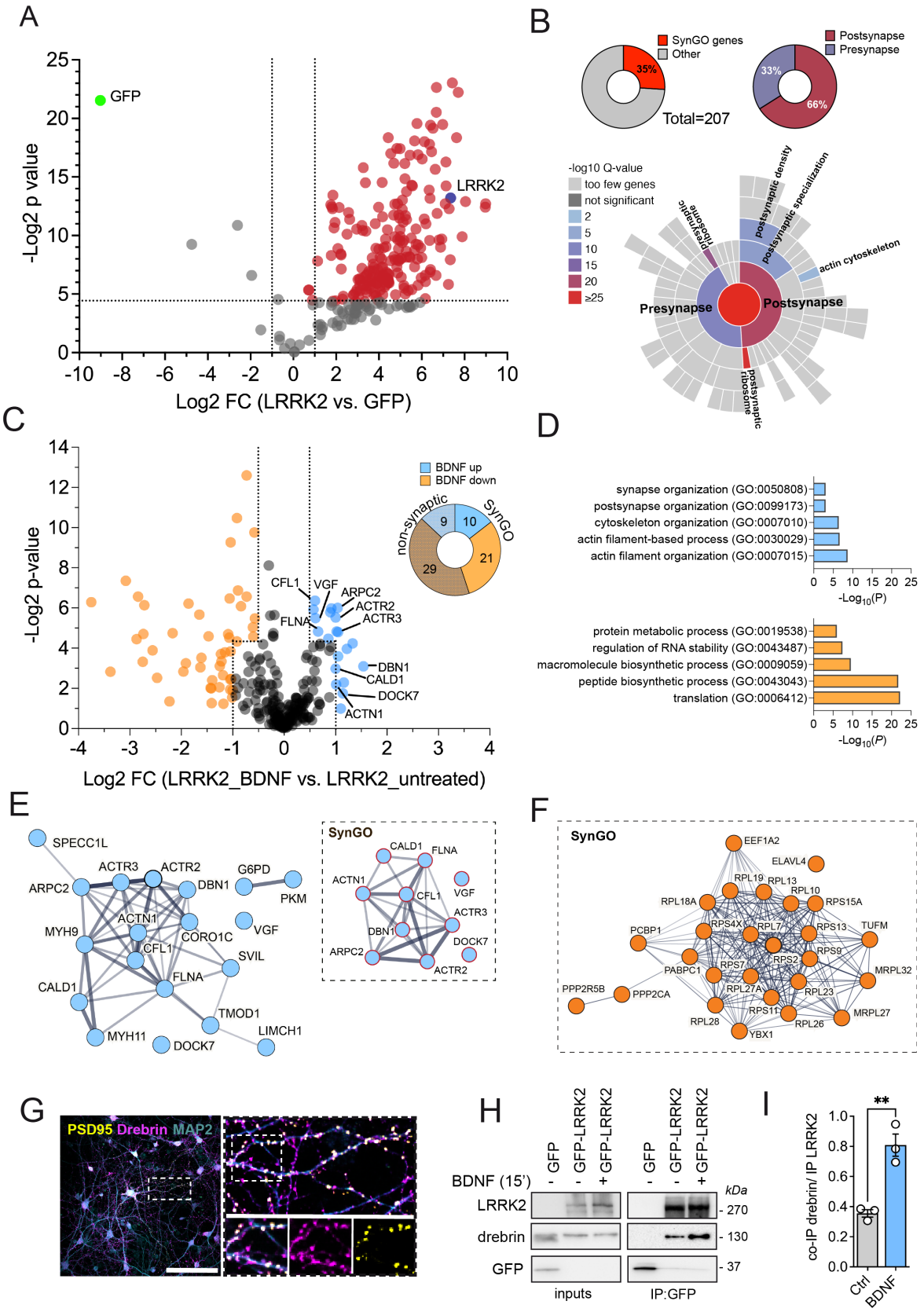

Figure 2. BDNF promotes LRRK2 interaction with post-synaptic actin cytoskeleton components.

(A) Volcano plot of GFP-LRRK2 versus GFP enriched interactors from differentiated SH-SY5Y cells (n=6 replicates: n=3 independent experiments each with 2 technical replicates). Interactors that were considered for SynGO analysis have adjusted *P* value < 0.05 and FC > 2. (red dots). **(B)** Donut charts with % of SynGO genes among the total 207 LRRK2 interactors (A) and with % of presynaptic and postsynaptic proteins among SynGO genes. SynGO-CC terms visualized with a sunburst plot showing significant categories (below). **(C)** Volcano plot of GFP-LRRK2 +/-BDNF enriched interactors from differentiated SH-SY5Y cells (n=6 replicates: n=3 independent experiments each with 2 technical replicates). Interactors selected for pathway enrichment analysis fall into two categories: (i) adjusted *P* value < 0.05 and FC > 0.5 | FC < -0.5 or (ii) FC > 1 | FC < -1. Proteins with increased interaction upon BDNF stimulation are blue-labeled, proteins with decreased interaction are orange-labeled. Donut chart showing the number of SynGO annotated genes versus non synaptic proteins in BDNF-up versus BDNF-down interactors (top right). **(D)** G:profiler g:GOSt pathway enrichment analysis showing the top enriched categories of BDNF-increased interactors (top, blue bar graph) versus BDNF-decreased interactors (bottom, orange bar graph). **(E)** Protein-Protein Interaction Networks built with STRING (https://string-db.org/) of all BDNF(+) interactors and SynGO BDNF-increased interactors (inset) and **(F)** of SynGO BDNF-decreased interactors. **(G)** Confocal immunofluorescence of DIV14 primary neurons co-stained with MAP2 (neuronal marker), PSD95 (postsynaptic marker) and drebrin. Scale bar: 100 µm; magnifications scale bar: 10 µm. **(H)** Validation of increased drebrin:LRRK2 interaction upon BDNF treatment (15 mins). Samples are the same analyzed in the three rounds of MS (A). **(I)** Quantification of (H).

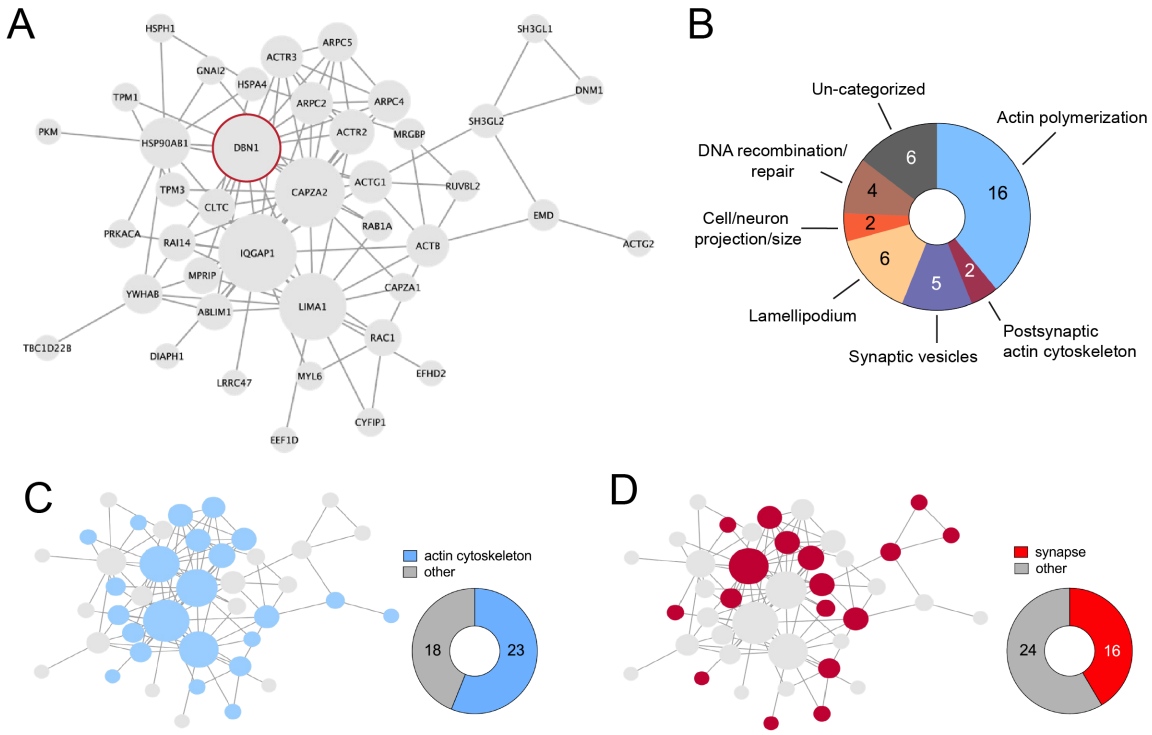

Figure 3. An actin-synaptic cluster from the LRRK2 protein-protein interaction network. **(A)** Network graph showing one of the topological clusters extracted from the LRRK2 protein-protein interaction network. Proteins are represented as nodes while protein-protein interactions are represented as edges. Node size is proportional to the degree centrality: the larger the node, the higher the degree, the more interactions the node has in the network. **(B)** Gene Ontology biological-processes (GO-BPs) enrichment; the analysis was performed using g:Profiler, GO-BPs with term size >500 were discarded as general terms and the remaining terms was clustered based on semantics using the keywords: Postsynaptic (Actin) Cytoskeleton, Lamellipodium, Synaptic Vesicle, Actin Polymerization/Nucleation, DNA Recombination/Repair, Cell/Neuron Projection. **(C)** Network graph as in (A) highlighting actin cytoskeletal proteins in blue and the proportion over the total (pie chart). (**D**) Network graph as in (A) highlighting synaptic proteins in red and the proportion over the total (pie chart).

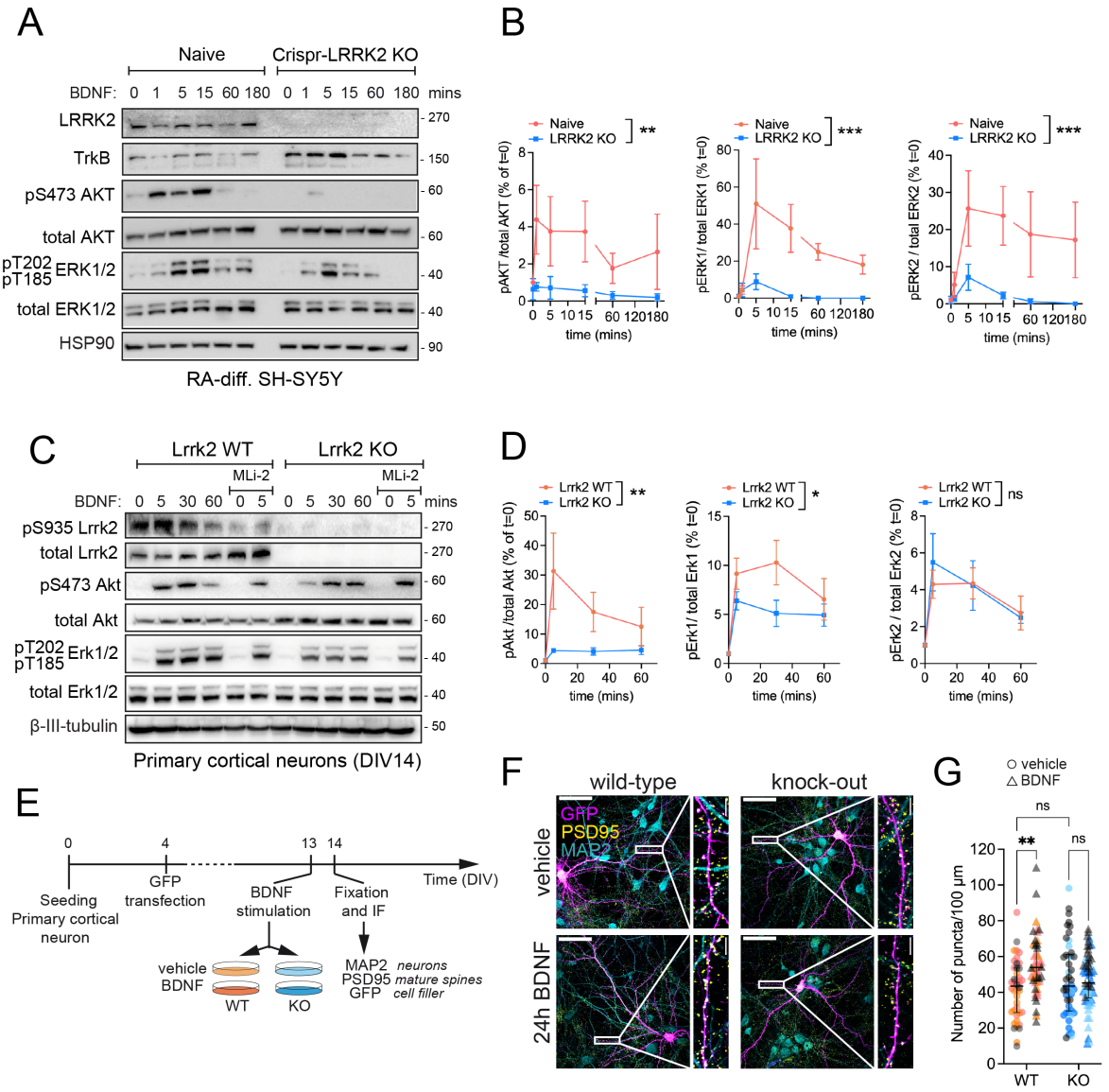

Figure 4. BDNF-induced spinogenesis is impaired in *Lrrk2* knockout neurons. (A) Six-day RA-differentiated SH-SY5Y naïve and CRISPR-LRRK2 KO cells stimulated with BDNF at different time points (0, 1, 5, 15, 60, 180 mins). Anti-TrkB antibodies were used to confirmed expression of BDNF receptor. To compare BDNF-induced signaling in naïve vs LRRK2-KO cells, phosphorylated Akt (S473) and Erk1/2 (T185/T202) were evaluated. **(B)** Quantification of phosphorylated proteins show from *n*=3 independent differentiation expeiments. Two-way ANOVA; phospho-Akt: interaction *P*=0.7079, F (5, 24) = 0.5896; genotype: ***P*=0.0014, F (1, 24) = 13.07; time: *P*=0.5610, F (5, 24) = 0.7994. Phospho-Erk1: interaction *P*=0.0783, F (5, 24) = 2.284; genotype: ****P*=0.0003, F (1, 24) = 17.58; time: **P*=0.0244, F (5, 24) = 3.174. Phospho-Erk2: interaction: *P*=0.3725, F (5, 24) = 1.128; genotype: ****P*=0.0008 F (1, 24) = 14.59; time: *P*=0.1356, F (5, 24) = 1.879. **(C)** DIV14 primary cortical neurons from WT vs KO mice stimulated with BDNF at different time points (0, 5, 15, 30, 60 mins) in the presence or

absence of LRRK2 inhibitor MLi-2 (90 min, 500 nM). To compare BDNF-induced signaling in WT vs KO neurons, phosphorylated Akt (S473) and Erk1/2 (T185/T202) were evaluated. Phosphorylated LRRK2 was assessed with pS935 antibodies. **(D)** Quantification of phosphorylated proteins show from n=9 independent cultures. Two-way ANOVA; phospho-Akt: interaction P=0.1186, F (3, 63) = 2.031; genotype: **P=0.0037, F (1, 63) = 9.101; time: P=0.0342, F (3, 63) = 3.069. Phospho-Erk1: interaction P=0.3256, F (3, 64) = 1.177; genotype: *P=0.0201, F (1, 64) = 5.680; time: ****P<0.0001, F (3, 64) = 10.04. Phospho-Erk2: interaction P=0.8524, F (3, 62) = 0.2622; genotype: P=0.7528, F (1, 62) = 0.1001; time: ***P=0.0003, F (3, 62) = 7.428. **(E)** Overview of the experimental workflow to induce spine formation/maturation. **(F)** Representative confocal images of primary cortical neurons stimulated with 100 ng/ml of BDNF or vehicle control for 24 hours. GFP has been transfected at DIV4 to fill the neuroplasm and visualize individual dendrites, MAP2 is a neuronal marker and PSD95 is a marker of mature spines. **(G)** Quantification of the number of PSD-positive puncta per unit of length (100 µm). Dots represents individual segments (n≅20 neurites from n=5-6 neurons per replicate) and colors define neuronal cultures prepared in different days from pulled pups (n≅8 pups per culture per genotype, n=3 independent cultures). Two-way ANOVA; interaction **P=0.0038, F (1, 191) = 8.584; genotype: P=0.5833, F (1, 191) = 0.3020; treatment: *P=0.0126, F (1, 191) = 6.346. Šídák's multiple comparisons test: vehicle vs. BDNF (WT) ***P=0.0005; vehicle vs. BDNF (KO) P=0.9440; Vehicle (WT) vs. vehicle (KO) P= 0.3756.

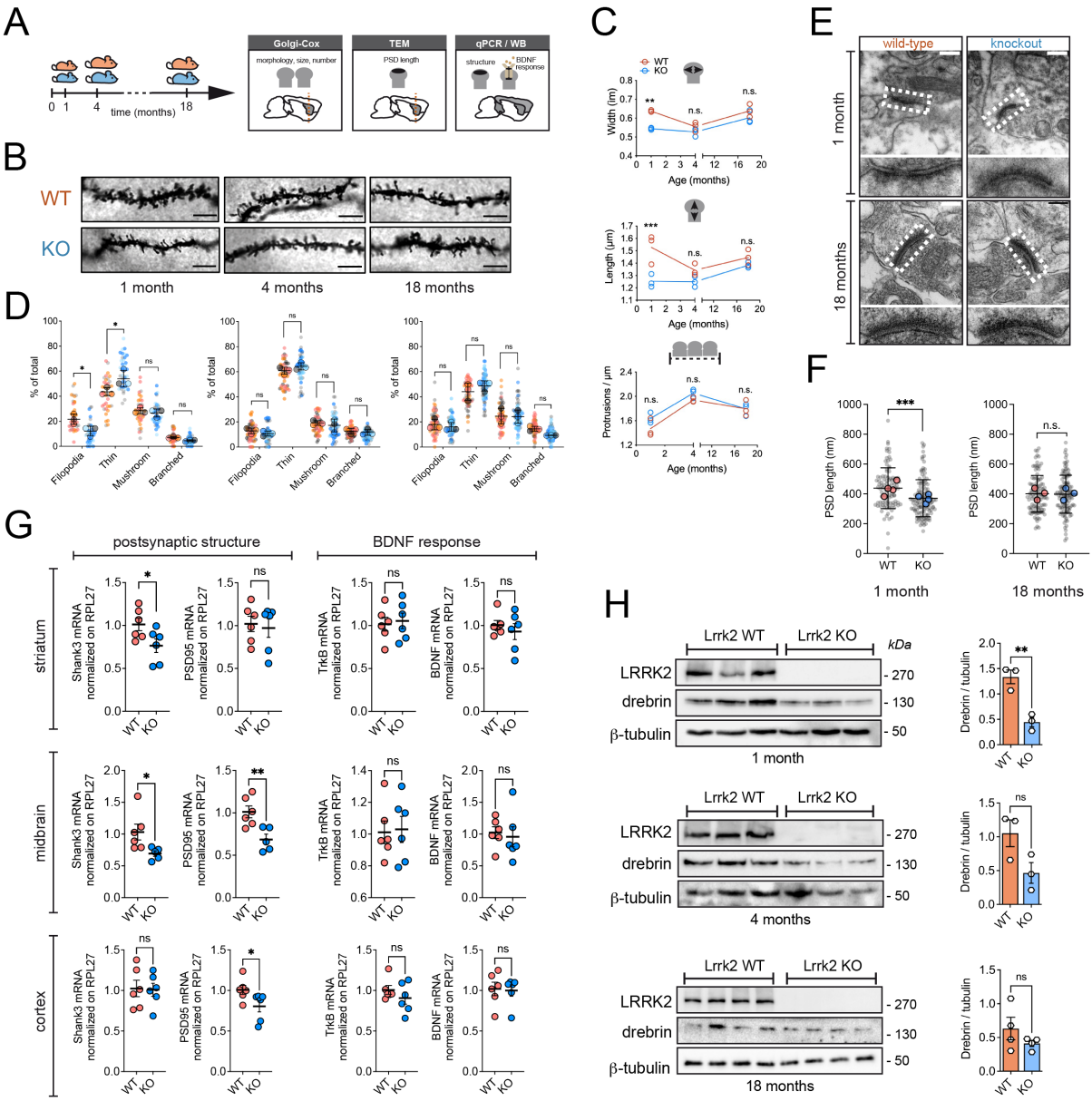

Figure 5. Striatal spine maturation is delayed in *Lrrk2* knockout mice.

(A) Overview of experimental design. **(B)** Representative images of neurite segments from Golgi-Cox stained neurons of dorsal striatum. Scale bar: 3 µm. **(C)** Quantification of average spine number (top), width (middle) and length (bottom) of *n*=3 animals per group (same segments analyzed in B). Statistical significance was determined by two-way ANOVA with Šídák's multiple comparisons test. Number of protrusions: interaction *P*=0.3820, F (2, 12) = 1.044; age: ****$P<0.0001$, F (2, 12) = 27.12; genotype: *P*=0.0840, F (1, 12) = 3.550; WT vs. KO (1 month) *P*=0.2013; WT vs. KO (4 months) *P*=0.5080; WT vs. KO (18 months) *P*>0.9999. Width: interaction *P*=0.0815, F (2, 12) = 3.112; age: ***$P=0.0004$, F (2, 12) = 16.14; genotype:

***P=0.0007, F (1, 12) = 20.77; WT vs. KO (1 month) **P=0.0017; WT vs. KO (4 months) P=0.4602; WT vs. KO (18 months) P=0.2489. Length: interaction *P=0.0345, F (2, 12) = 4.514; age: *P=0.0203, F (2, 12) = 5.488; genotype: ***P=0.0006, F (1, 12) = 21.53; WT vs. KO (1 month) ***P=0.0008; WT vs. KO (4 months) P=0.2875; WT vs. KO (18 months) P=0.5948. **(D)** Morphological classification of protrusions into four classes (filopodia, thin, mushroom, branched) and quantified as % of the total number. Each dot represents one segment ($n \geq 20$ segments analyzed per animal; genotype: wild-type vs. *Lrrk2* KO; age: 1, 4, 18 month-old; n=3 mice per group) and error bars represent the mean ± SD of n=3 mice (color coded). Statistical significance was determined by two-way ANOVA with Šídák's multiple comparisons test on mean values. One-month: interaction: **P=0.0017, F (3, 16) = 8.018; genotype: P=0.5731, F (1, 16) = 0.3309; class of protrusion: ****P<0.0001, F (3, 16) = 158.4; filopodia WT vs. KO P=0.0201; thin WT vs. KO *P=0.0102; mushroom WT vs. KO P=0.9585; branched WT vs. KO P=0.8726. Four-months: interaction: P=0.3178, F (3, 16) = 1.271; genotype: P=0.7300, F (1, 16) = 0.1233; class of protrusion: ****P<0.0001, F (3, 16) = 438.9; filopodia WT vs. KO P=0.8478; thin WT vs. KO P=0.4921; mushroom WT vs. KO P=0.8882; branched WT vs. KO P=0.9858. Eighteen-months: interaction: P=0.3237, F (3, 16) = 1.253; genotype: P=0.6880, F (1, 16) = 0.1672; class of protrusion: ****P<0.0001, F (3, 16) = 69.67; filopodia WT vs. KO P=0.9756; thin WT vs. KO P=0.6413; mushroom WT vs. KO P>0.9999; branched WT vs. KO P=0.5290. **(E)** Representative transmission electron microscopy (TEM) micrographs of striatal synapses from 1-month and 18-month old WT vs KO mouse brain slices (n=3-4 mice per genotype). Scale bar: 200 nm. **(F)** Quantification of post-synaptic density (PSD) length. Graphs show the length of individual synapses (grey dots) and the average PSD length per animal (colored dots). Statistical significance has been calculated with Student's t-test: 1 month-old mice (n=4 mice, 95 synapses WT, 118 synapses KO, ***P=0.0003); 18-month old mice (n=3 mice, 108 synapses WT, 119 synapses KO, P=0.8502). **(G)** Quantitative PCR of *Bdnf, TrkB, Psd95* and *Shank3* mRNA expression in striatum, cortex and midbrain form n=6 *Lrrk2* WT and n=6 *Lrrk2* KO one-month old mice. Statistical significance has been calculated with Student's t-test. (**H**) Western blot analysis of brain samples from the same Lrrk2 WT and KO mice where Golgi-Cox staining has been performed. The reduction in drebrin content is significant in Lrrk2 KO mice at 1 month of age. Differences between the two genotypes have been evaluated using Student's t-test (significance **P<0.01), n=3 animals per genotype per age.

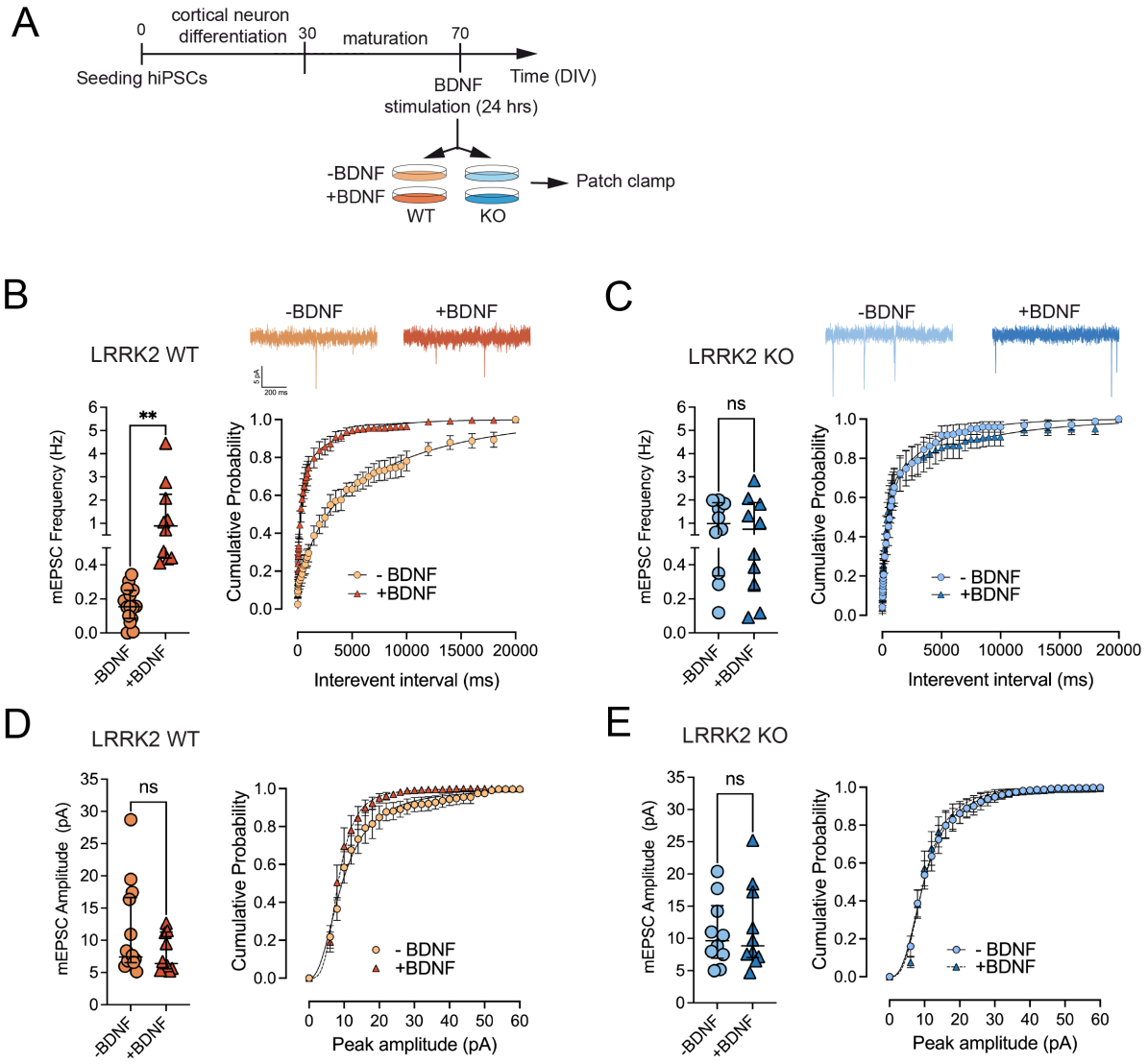

Figure 6. Effect of BDNF exposure on spontaneous electrical activity recorded in LRRK2 WT and KO cortical neurons. (**A**) Schematic representation of the experimental setup. (**B**) Representative spontaneous traces of hiPSC-derived cortical neurons WT in the presence or absence of 50 ng/ml BDNF for 24 hrs (upper). Left plot: frequency of mini postsynaptic excitatory currents (mEPSC) in LRRK2 WT (vehicle: 0.16 ± 0.03 Hz (n=15, N=3); BDNF: 1.36 ± 0.38 Hz (n=11, N=3). Statistical significance was determined using Student's paired t-test (LRRK2 WT: vehicle vs. BDNF $^{**}P < 0.01$; LRRK2 KO: vehicle vs. BDNF $P > 0.05$). Right plot: cumulative probability curves of interevent interval (IEIs) in WT -/+ BDNF treatment. (**C**) Representative spontaneous traces of hiPSC-derived cortical neurons KO in the presence or absence of 50 ng/ml BDNF for 24 hrs (upper). Left plot: frequency of mini postsynaptic excitatory currents (mEPSC) in LRRK2 KO (vehicle: 1.09 ± 0.21 Hz (n=11, N=3);

BDNF: 1.11 ± 0.25 Hz (*n*=12, *N*=3). Statistical significance was determined using Student's paired t-test (LRRK2 KO: vehicle vs. BDNF $P > 0.05$). Right plot: cumulative probability curves of interevent interval (IEIs) in KO -/+ BDNF treatment. (**D**) Left plot: amplitude of mini postsynaptic excitatory currents (mEPSC) in LRRK2 WT. BDNF treatment has no effect on the average peak amplitude (vehicle: 11.00 ± 1.85 pA (*n*=14, *N*=3); BDNF: 7.4 ± 0.77 pA (*n*=10, *N*=3)). Statistical significance was determined using Student's paired t-test (vehicle vs. BDNF $P > 0.05$). Right plot: cumulative probability curves of peak amplitude in WT -/+ BDNF treatment. (**E**) Left plot: amplitude of mini postsynaptic excitatory currents (mEPSC) in LRRK2 KO. BDNF treatment has no effect on the average peak amplitude (vehicle 10.42 ± 1.53 pA (*n*=11, *N*=3), BDNF 11.12 ± 1.76 pA (*n*=12, *N*=3)). Statistical significance was determined using Student's paired t-test (vehicle vs. BDNF $P > 0.05$). Right plot: cumulative probability curves of peak amplitude in WT -/+ BDNF treatment.

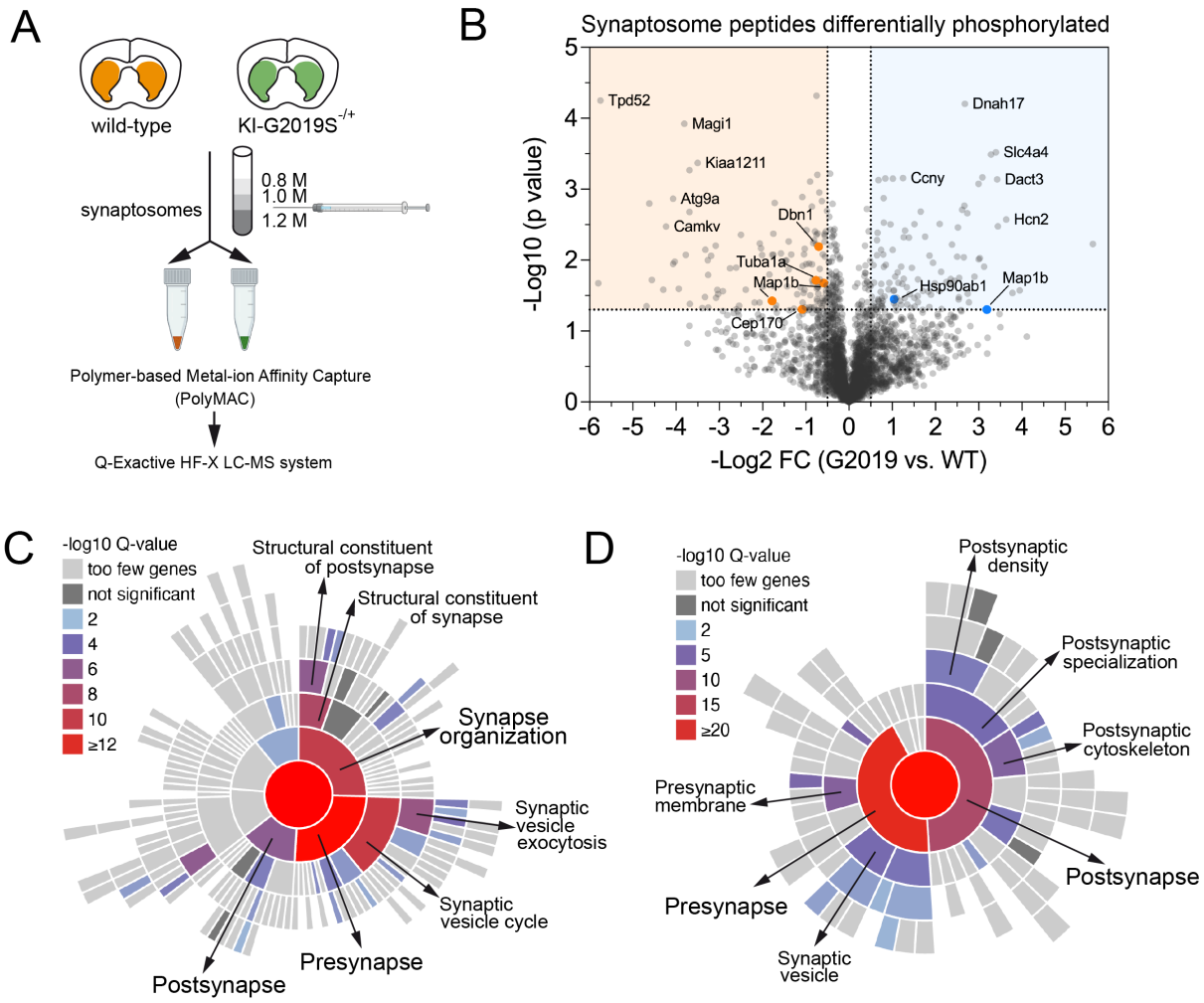

Figure 7. Phosphoproteome of Lrrk2^{G2019S} synaptosomes is enriched in postsynaptic structure organization SynGO terms.

(A) Overview of experimental design. **(B)** Volcano plot of 2957 differentially phosphopeptides common between WT and Lrrk2^{G2019S} striatal synaptosomes (labeled with gene name) isolated from Lrrk2 WT and Lrrk2^{G2019S} KI mice. Common genes between this analysis and the AP-MS analysis are orange labelled for peptides with decreased phosphorylation and blue labelled for peptides with increased phosphorylation. **(C)** Sunburst plot showing enriched SynGO biological processes (BP) categories (267 proteins, at least one significant peptide, $P < 0.05$ and fold change > 0.5). **(D)** Sunburst plot showing enriched SynGO cellular component (CC) categories (267 proteins, at least one significant peptide, $P < 0.05$ and fold change > 0.5).